Controllability and stability analysis of planar snake robot locomotion

Pål Liljebäck, *Member, IEEE,* Kristin Y. Pettersen, *Senior Member, IEEE,* Øyvind Stavdahl, *Member, IEEE,* and Jan Tommy Gravdahl, *Senior Member, IEEE*

***Abstract*—This paper contributes to the understanding of snake robot locomotion by employing nonlinear system analysis tools for investigating fundamental properties of snake robot dynamics. The paper has five contributions: 1) A partially feedback linearized model of a planar snake robot influenced by viscous ground friction is developed. 2) A stabilizability analysis is presented proving that any asymptotically stabilizing control law for a planar snake robot to an equilibrium point must be *time-varying*. 3) A controllability analysis is presented proving that planar snake robots are *not* controllable when the viscous ground friction is *isotropic*, but that a snake robot becomes *strongly accessible* when the viscous ground friction is *anisotropic*. The analysis also shows that the snake robot does *not* satisfy sufficient conditions for *small-time local controllability* (STLC). 4) An analysis of snake locomotion is presented that easily explains how anisotropic viscous ground friction enables snake robots to locomote forward on a planar surface. The explanation is based on a simple mapping from link velocities normal to the direction of motion into propulsive forces in the direction of motion. 5) A controller for straight line path following control of snake robots is proposed and a *Poincaré map* is investigated to prove that the resulting state variables of the snake robot, except for the position in the forward direction, trace out an exponentially stable periodic orbit.**

***Index Terms*—Biologically-Inspired Robots, Underactuated Robots, Snake Robot, Motion Control, Poincaré maps.**

I. Introduction

INSPIRED by biological snake locomotion, snake robots carry the potential of meeting the growing need for robotic mobility in unknown and challenging environments. These mechanisms typically consist of serially connected joint modules capable of bending in one or more planes. The many degrees of freedom of snake robots make them difficult to control, but they provide traversability in irregular environments that surpasses the mobility of the more conventional wheeled, tracked and legged forms of robotic mobility. Research on snake robots has been conducted for several decades. However, our understanding of snake locomotion so far is for the most part based on empirical studies of biological snakes and simulation-based synthesis of relationships between parameters of the snake robot. This paper is an attempt to contribute to the understanding of snake robots by employing nonlinear system analysis tools for investigating fundamental properties of their dynamics.

There are several reported works aimed at analysing and understanding snake locomotion. Gray [1] conducted empirical and analytical studies of snake locomotion already in the 1940s. Hirose [2] studied biological snakes and developed mathematical relationships characterizing their motion, such as the *serpenoid curve*. Ostrowski [3] studied the controllability properties of a wheeled snake robot on a purely kinematic level. Prautsch *et al.* [4] modelled the dynamics of a wheeled snake robot and proposed an asymptotically stable controller for the position of the robot. Ma [5] modelled a planar snake robot without wheels and optimized the motion of the robot based on computer simulations. Date *et al.* [6] developed controllers for wheeled snake robots aimed at minimizing the lateral constraint forces on the wheels of the robot during locomotion. Saito *et al.* [7] modelled a planar snake robot and optimized the parameters of Hirose's serpenoid curve based on simulations. Hicks [8] investigated general requirements for the propulsion of a three-linked snake robot. Nilsson [9] employed energy arguments to analyse planar snake locomotion with isotropic friction. Transeth *et al.* [10] proved that the translational and rotational velocity of a planar snake robot is bounded. Li *et al.* [11] studied the controllability of the joint motion of a snake robot, but they did not consider the position and orientation of the robot. Ishikawa [12] proposed feedback control strategies (on a kinematic level) for a three-linked wheeled snake robot based on Lie bracket calculations and employed Poincaré maps to study the motion of the robot.

Research on control of robotic fish and eel-like mechanisms is relevant to research on snake robots since these mechanisms are very similar. The works in [13]–[15] investigate the controllability of various fish-like mechanisms, synthesize gaits for translational and rotational motion based on Lie bracket calculations, and propose controllers for tracking straight and curved trajectories.

This paper is based on results previously presented by the authors in [16] and [17], and provides five distinct contributions. The first contribution is a partially feedback linearized model of a planar snake robot that builds on a model previously presented in [18]. This approach resembles the work in [11]. However, the feedback linearized model in [11] does not include the position of the snake robot, which is a key ingredient in this paper.

The second contribution is a stabilizability analysis for planar snake robots that proves that any asymptotically stabilizing

Manuscript received January 26, 2010.

Affiliation of Pål Liljebäck is shared between the Dept. of Engineering Cybernetics at the Norwegian University of Science and Technology (NTNU), NO-7491 Trondheim, Norway, and SINTEF ICT, Dept. of Applied Cybernetics, N-7465 Trondheim, Norway. E-mail: Pal.Liljeback@sintef.no.

Kristin Y. Pettersen, Øyvind Stavdahl, and Jan Tommy Gravdahl are with the Dept. of Engineering Cybernetics at the Norwegian University of Science and Technology (NTNU), NO-7491 Trondheim, Norway. E-mail: {Kristin.Y.Pettersen, Oyvind.Stavdahl, Tommy.Gravdahl}@itk.ntnu.no.

control law for a planar snake robot to an equilibrium point must be *time-varying*, i.e. not of pure-state feedback type (see Theorem 3). This result is valid regardless of which type of ground friction the snake robot is subjected to.

The third contribution is a controllability analysis for planar snake robots influenced by viscous ground friction forces. The analysis shows that a snake robot is *not* controllable when the viscous ground friction is *isotropic* (see Theorem 5), but that a snake robot becomes *strongly accessible* when the viscous ground friction is *anisotropic* (see Theorem 6). The analysis also shows that the snake robot does *not* satisfy sufficient conditions for *small-time local controllability* (see Theorem 8). To the authors' best knowledge, no formal controllability analysis has previously been reported for the position and link angles of a wheelless snake robot influenced by ground friction. Note that the work in [11] studies the controllability of the joints of a snake robot under the assumption that one joint is passive. However, the analysis does not consider the position of the snake.

The fourth contribution is the development of a simple relationship between link velocities *normal* to the direction of motion and *propulsive forces* in the direction of motion. This relationship explains how snake robots influenced by anisotropic ground friction are able to locomote forward on a planar surface. To the authors' best knowledge, previously published research on snake robots has not presented an explicit mathematical description that *easily* explains how a snake robot achieves forward propulsion.

Finally, the fifth contribution is a path following controller that enables snake robots to track a planar straight path, and the use of a *Poincaré map* to study the stability properties of the motion along the path. The method of *Poincaré maps* [19] represents a widely used tool for proving the existence and stability of periodic orbits of dynamical systems (see e.g. [20]). In this paper, a *Poincaré map* is employed to prove that all state variables of the snake robot, except for the position in the forward direction, trace out an *exponentially stable* periodic orbit when the proposed controller is applied.

The paper is organized as follows. Section II introduces some selected tools for analyzing controllability of nonlinear systems. Section III gives an introduction to Poincaré maps. Section IV presents a mathematical model of a planar snake robot. Section V converts the model to a simpler form through partial feedback linearization. Section VI and Section VII studies, respectively, the stabilizability and controllability properties of planar snake robots. Section VIII explains how snake robots are able to move forward. Section IX proposes a controller for the snake robot. Section X investigates the stability of the proposed controller based on a Poincaré map. Finally, Section XI presents concluding remarks.

II. Introduction to nonlinear controllability analysis

This section presents a brief summary of selected tools for analyzing the controllability of nonlinear systems. The summary given below is formulated in an intuitive form that aims to be easily understandable for readers unaccustomed with nonlinear controllability analysis. For a rigorous presentation, the readers are referred to [21]–[23].

Analyzing the controllability of a *linear* system is straightforward and involves a simple test (the *Kalman rank condition* [21]) on the constant system matrices. However, studying the controllability of a *nonlinear* system is far more complex and constitutes an active area of research. In the following, we summarize important controllability concepts for control-affine nonlinear systems, i.e. systems of the form

$$\dot{x} = f(x) + \sum_{j=1}^{m} g_j(x)\, v_j, \quad x \in \mathbb{R}^n, \quad v \in \mathbb{R}^m \tag{1}$$

where the vector fields of the system are the drift vector field, $f(x)$, and the control vector fields, $g_j(x)$, $j \in \{1, .., m\}$.

A nonlinear system is said to be *controllable* if there exist admissible control inputs that will move the system between two arbitrary states in finite time. However, conditions for this kind of controllability that are both necessary and sufficient do not exist. Nonlinear controllability is instead typically analyzed by investigating the local behaviour of the system near equilibrium points.

The simplest approach to studying controllability of a nonlinear system is to linearize the system about an equilibrium point, x^e. If the linearized system satisfies the Kalman rank condition at x^e, the nonlinear system is controllable in the sense that the set of states that can be reached from x^e contains a neighborhood of x^e [21]. Unfortunately, many underactuated systems do not have a controllable linearization. Moreover, a nonlinear system can be controllable even though its linearization is not.

A necessary (but not sufficient) condition for controllability from a state x_0 (not necessarily an equilibrium) is that the nonlinear system satisfies the *Lie algebra rank condition* (LARC), also called the *accessibility rank condition* [21]. If this is the case, the system is said to be *locally accessible* from x_0. This property means that the space that the system can reach within any time $T > 0$ is fully n-dimensional, i.e. the reachable space from x_0 has a dimension equal to the dimension of the state space. A slightly stronger property is *strong accessibility*, which means that the space that the system can reach in *exactly* time T for any $T > 0$ is fully n-dimensional.

Accessibility of a nonlinear system is investigated by computing the *accessibility algebra*, here denoted Δ, of the system. Computation of Δ requires knowledge of the *Lie bracket* [21], which is now briefly explained. The drift and control vector fields of the nonlinear system (1) indicate directions in which the state x can move. These directions will generally only span a subset of the complete state space. However, through combined motion along two or more of these vector fields, it is possible for the system to move in directions not spanned by the original system vector fields. The Lie bracket between two vector fields Y and Z produces a new vector field defined as $[Y, Z] = \frac{\partial Z}{\partial x} Y - \frac{\partial Y}{\partial x} Z$. When Y and Z are any of the system vector fields, the Lie bracket $[Y, Z]$ *approximates* the net motion produced when the system follows these two vector fields in an alternating fashion. The classical example is parallel parking with a car, where sideways motion of

the car may be achieved through an alternating turning and forward/backward motion. Note that Lie brackets can be computed from other Lie brackets, thereby producing nested Lie brackets. The *accessibility algebra*, Δ, is a set of vector fields composed of the system vector fields, f and g_j, the Lie brackets between the system vector fields, and also higher order Lie brackets generated by nested Lie brackets. The LARC is satisfied at x_0 if the vector fields in $\Delta(x_0)$ span the entire n-dimensional state space ($\dim(\text{span}(\Delta)) = n$). The following result is proved in [21]:

Theorem 1: The system (1) is *locally accessible* from x_0 if and only if the LARC is satisfied at x_0. The system is *locally strongly accessible* if the drift field f by itself (i.e. unbracketed) is not included in the *accessibility algebra*.

Accessibility does *not* imply controllability since it only infers conclusions on the dimension of the reachable space from x_0. Accessibility is, however, a necessary (but not sufficient) condition for *small-time local controllability* (STLC) [22]. STLC is desirable since it is in fact a stronger property than controllability. If a system is STLC, then the control input can steer the system in any direction in an arbitrarily small amount of time. For second-order systems, STLC is only considered from equilibrium states since it is generally not possible for a second-order system to instantly move in one direction if it already has a velocity in the opposite direction.

Sussmann presented sufficient conditions for STLC in [22]. These results were later extended by Bianchini and Stefani [23]. We now summarize these conditions. For any Lie bracket term B generated from the system vector fields, define the θ-degree of B, denoted $\delta_\theta(B)$, and the l-degree of B, denoted $\delta_l(B)$, as

$$\delta_\theta(B) = \frac{1}{\theta}\delta^0(B) + \sum_{j=1}^{m}\delta^j(B) \;\;,\;\; \delta_l(B) = \sum_{j=0}^{m} l_j \delta^j(B) \qquad (2)$$

respectively, where $\delta^0(B)$ is the number of times the drift vector field f appears in the bracket B, $\delta^j(B)$ is the number of times the control vector field g_j appears in the bracket B, θ is an arbitrary number satisfying $\theta \in [1, \infty)$, and l_j is an arbitrary number satisfying $l_j \geq l_0 \geq 0$, $\forall\, j \in \{0, .., m\}$. The bracket B is said to be *bad* if $\delta^0(B)$ is odd and $\delta^1(B), ..., \delta^m(B)$ are all even. A bracket is *good* if it is not bad. As an example, we have that the bracket $[g_j, [f, g_k]]$ is *bad* for $j = k$ and *good* for $j \neq k$. This classification is motivated by the fact that a bad bracket *may* have directional constraints. E.g. the drift vector f is *bad* because it only allows motion in its positive direction and not in its negative direction, $-f$. A bad bracket is said to be *θ-neutralized* (resp. *l-neutralized*) if it can be written as a linear combination of good brackets of lower θ-degree (resp. l-degree). The *Sussmann condition* and the *Bianchini and Stefani condition* for STLC are now combined in the following theorem:

Theorem 2: The system (1) is *small-time locally controllable* (STLC) from an equilibrium point x^e ($f(x^e) = 0$) if the LARC is satisfied at x^e and either all *bad* brackets are *θ-neutralized* (Sussmann [22]) or all *bad* brackets are *l-neutralized* (Bianchini and Stefani [23]).

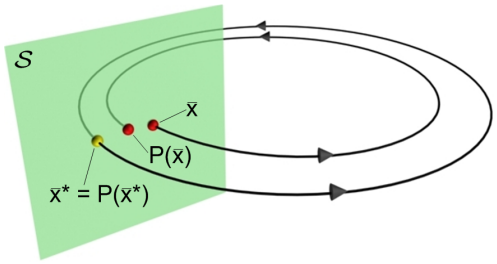

Fig. 1. Illustration of the Poincaré map corresponding to a Poincaré section $\mathcal{S}$.

III. Introduction to Poincaré maps

This section gives a brief presentation of the *Poincaré map* since this is used as a stability analysis tool in Section X. For further details on the topic, the reader is referred to [19] and [20].

A. General description of Poincaré maps

The *Poincaré map* represents a widely used tool for analysing the existence and stability of periodic orbits of dynamical systems. Consider an autonomous (not explicitly dependent on time) n-dimensional dynamical system of the form

$$\dot{x} = f(x), \quad x \in \mathbb{R}^n \qquad (3)$$

where $f(x)$ is assumed to be *continuously differentiable.* Assume that the solution of this differential equation for a particular initial condition is a *limit cycle*. This means that the flow of x in the n-dimensional state space will return to the initial condition after a time T, corresponding to the period of the limit cycle.

We now define an $(n-1)$-dimensional hyperplane $\mathcal{S}$ (called a *Poincaré section*) such that the limit cycle intersects and passes through $\mathcal{S}$ at some instant in time. We denote by $\overline{x} \in \mathbb{R}^{n-1}$ the $(n-1)$-dimensional state vector when x is constrained to $\mathcal{S}$. The point on $\mathcal{S}$ where the limit cycle intersects $\mathcal{S}$ is denoted $\overline{x}^* \in \mathbb{R}^{n-1}$. Assume now that we initialize (3) on the hyperplane $\mathcal{S}$ somewhere close to $\overline{x}^*$. Due to the continuity of the solutions of (3) with respect to the initial condition, the flow of x will, in approximately T seconds, return to and intersect S somewhere close to $\overline{x}^*$. This is illustrated in Fig. 1. The mapping from an initial point $\overline{x}$ on $\mathcal{S}$ to the next point where the flow of x intersects $\mathcal{S}$ is called the *Poincaré map* and is denoted by $P(\overline{x}) \in \mathbb{R}^{n-1}$. The Poincaré map is in other words a function that accepts an initial point on a Poincaré section as input and outputs where the Poincaré section will be intersected next by the flow of x. This is written more formally as $P : \mathcal{S} \to \mathcal{S}$. The point $\overline{x}^*$ is called a *fixed point* of the Poincaré map since the Poincaré map maps $\overline{x}^*$ back to itself. This is also illustrated in Fig. 1. We only consider *one-sided* Poincaré maps, i.e. we only consider crossings of $\mathcal{S}$ in directions corresponding to the direction of $\dot{x}$ when x initially left $\mathcal{S}$.

The Poincaré map can be interpreted as a *discrete-time* system with an $(n-1)$-dimensional state space that evolves on the Poincaré section. This is seen by denoting by $\overline{x}[k] \in \mathcal{S}$

the point of the k-th intersection with $\mathcal{S}$ by the flow of x. The Poincaré map may then be written as

$$\overline{x}\left[k+1\right] = P\left(\overline{x}\left[k\right]\right), \quad \overline{x}\left[0\right] \in \mathcal{S}. \tag{4}$$

The usefulness of the Poincaré map for stability analysis lies in the fact that *local exponential stability* of the fixed point $\overline{x}^*$ on the Poincaré section is equivalent to *local exponential stability* of the underlying periodic orbit [20], i.e. nearby orbits converge exponentially to the periodic orbit. Note that the stability is only *asymptotic* (i.e. not *exponential*) if $f(x)$ in (3) is *continuous* but not *continuously differentiable* [20]. The problem of determining if a periodic orbit of the system (3) is exponentially stable is, in other words, reduced to determining if $\overline{x}^*$ is an exponentially stable equilibrium point of the *discrete-time* system in (4), which is a much simpler problem to solve. A significant drawback of Poincaré maps is that they provide little insight into properties of the system dynamics.

Note that the method of Poincaré maps may also be applied to *non-autonomous* periodic systems, i.e. systems of the form $\dot{x} = f(x,t)$, by incapsulating the time t in an augmented periodic state variable $\beta = 2\pi t/T$. This is performed for the snake robot in Section X-A.

B. Practical application of Poincaré maps

This section provides an informal description of the practical use of Poincaré maps. The aim is to show how this method can be employed in practice in order to investigate the stability properties of a time-periodic dynamical system.

1) Calculating the Poincaré map: It is difficult to determine the Poincaré map analytically since it requires the solution of the differential equation (3). However, the Poincaré map of (3) is simply the forward integration of this differential equation. It is therefore possible to compute the Poincaré map $P(\overline{x}_0)$ numerically by initializing (3) on $\mathcal{S}$ at $\overline{x}_0$ and simulating (3) until $\mathcal{S}$ is intersected. The state corresponding to this intersection is the Poincaré map $P(\overline{x}_0)$.

2) Locating fixed points of the Poincaré map: The easiest way of locating a fixed point $\overline{x}^*$ of the Poincaré map is to simply let the simulation of (3) run until it reaches the steady state. This is called the *brute-force approach* and has three serious disadvantages. First of all, convergence to the fixed point can be exceedingly slow. Secondly, the method can only locate stable fixed points. Thirdly, it may be difficult to tell when the steady state has been reached.

A more sophisticated method is to exploit the fact that locating $\overline{x}^*$ is equivalent to locating zeros of the error function

$$E(\overline{x}) = P(\overline{x}) - \overline{x}, \quad E(\overline{x}) \in \mathbb{R}^{n-1} \tag{5}$$

since we have that $\overline{x}^* = P(\overline{x}^*)$. The *Newton-Raphson algorithm* [19] is a general algorithm for locating zeros of a differentiable function, and it may therefore be employed for locating $\overline{x}^*$. By starting from an inital guess, $\overline{x}^k$, of the fixed point, the *Newton-Raphson algorithm* calculates a more accurate estimate of $\overline{x}^*$ through the formula

$$\overline{x}^{k+1} = \overline{x}^k - J_E\left(\overline{x}^k\right)^{-1} E\left(\overline{x}^k\right) \tag{6}$$

where

$$J_E = \frac{\partial E}{\partial \overline{x}} = \begin{bmatrix} \frac{\partial E_1}{\partial \overline{x}_1} & \cdots & \frac{\partial E_1}{\partial \overline{x}_{n-1}} \\ \vdots & \ddots & \vdots \\ \frac{\partial E_{n-1}}{\partial \overline{x}_1} & \cdots & \frac{\partial E_{n-1}}{\partial \overline{x}_{n-1}} \end{bmatrix} \in \mathbb{R}^{(n-1)\times(n-1)} \tag{7}$$

is the Jacobian of the error function $E(\overline{x})$. The Jacobian $J_E\left(\overline{x}^k\right)$ can be calculated numerically by defining

$$d\overline{x}_i = \begin{bmatrix} 0 & \cdots & 0 & \Delta_i & 0 & \cdots & 0 \end{bmatrix}^T \in \mathbb{R}^{n-1} \tag{8}$$

where the i-th element is non-zero, and Δ_i is a *small perturbation* of $\overline{x}_i$ *along* S. Column i of $J_E\left(\overline{x}^k\right)$ may then be approximated numerically as

$$\frac{\partial E}{\partial \overline{x}_i}\left(\overline{x}^k\right) \approx \frac{E\left(\overline{x}^k + d\overline{x}_i\right) - E\left(\overline{x}^k\right)}{\Delta_i}. \tag{9}$$

This enables a column-wise construction of $J_E\left(\overline{x}^k\right)$. If the initial condition is within the basin of attraction of a periodic orbit, the *Newton-Raphson algorithm* will converge rapidly towards the fixed point $\overline{x}^*$.

3) Analysing stability of a periodic orbit: As explained in Section III-A, a fixed point $\overline{x}^*$ of the Poincaré map corresponds to a periodic orbit of the underlying dynamical system. Once the fixed point has been found using e.g. the *Newton-Raphson algorithm*, the stability of the periodic orbit may be tested by investigating if the fixed point is a stable equilibrium point of the Poincaré map. This is done by calculating the Jacobian linearization of the Poincaré map about the fixed point, i.e. by calculating the Jacobian $J_P(\overline{x}^*) = \frac{\partial P}{\partial \overline{x}}\big|_{\overline{x}=\overline{x}^*} \in \mathbb{R}^{(n-1)\times(n-1)}$. $J_P(\overline{x}^*)$ is calculated by following the same procedure as for calculating $J_E\left(\overline{x}^k\right)$ in (7). The Poincaré map linearized about the fixed point is thereby given as $\overline{x}\left[k+1\right] = J_P(\overline{x}^*)\,\overline{x}\left[k\right]$. This is a linear discrete-time system which is *exponentially stable* if the magnitude of all the eigenvalues of $J_P(\overline{x}^*)$ are strictly less than one. The fixed point $\overline{x}^*$ of the Poincaré map, and thereby also the periodic orbit of the underlying dynamical system, is therefore *locally exponentially stable* if the magnitude of all the eigenvalues of $J_P(\overline{x}^*)$ are strictly less than one.

IV. A MODEL OF THE SNAKE ROBOT

This section summarizes a mathematical model of a planar snake robot. For a more detailed presentation of this model, the reader is referred to [18]. A feedback linearized form of this snake robot model is developed in Section V in order to simplify the controllability analysis presented in Section VII.

A. Notations and defined symbols

The snake robot consists of n links of length $2l$ interconnected by $n-1$ joints. All n links have the same mass m and moment of intertia $J = \frac{1}{3}ml^2$. The total mass of the snake robot is therefore nm. The mass of each link is uniformly distributed so that the link CM (center of mass) is located at its center point (at length l from the joint at each side). The mathematical symbols defined in order to represent the kinematics and dynamics of the snake robot are described in Table I and illustrated in Fig. 2 and Fig. 3.

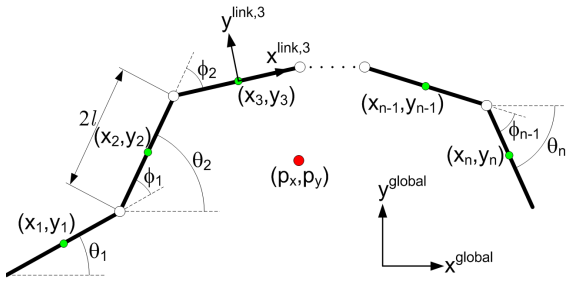

Fig. 2. Kinematic parameters for the snake robot.

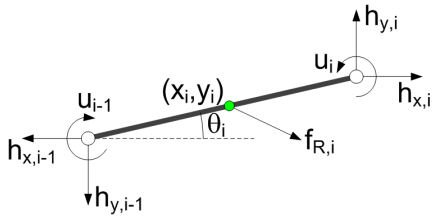

Fig. 3. Forces and torques acting on each link of the snake robot.

Vectors are either expressed in the global coordinate system or in the local coordinate system of link i. This is indicated by superscript *global* or *link*, i, respectively. If not otherwise specified, a vector with no superscript is expressed in the global coordinate system.

The following vectors and matrices are used in the subsequent sections:

Symbol	Description	Associated vector
n	Number of links.	
l	Half the length of a link.	
m	Mass of a link.	
J	Moment of inertia of a link.	
θ_i	Angle between link i and global x axis.	$\theta \in \mathbb{R}^n$
ϕ_i	Angle of joint i.	$\phi \in \mathbb{R}^{n-1}$
(x_i, y_i)	Global coordinates of CM of link i.	x, $y \in \mathbb{R}^n$
(p_x, p_y)	Global coordinates of the CM of the snake robot.	$p \in \mathbb{R}^2$
u_i	Actuator torque exerted on link i from link $i+1$.	$u \in \mathbb{R}^{n-1}$
u_{i-1}	Actuator torque exerted on link i from link $i-1$.	$u \in \mathbb{R}^{n-1}$
$f_{R,x,i}$	Friction force on link i in x direction.	$f_{R,x} \in \mathbb{R}^n$
$f_{R,y,i}$	Friction force on link i in y direction.	$f_{R,y} \in \mathbb{R}^n$
$h_{x,i}$	Joint constraint force in x direction on link i from link $i+1$.	$h_x \in \mathbb{R}^{n-1}$
$h_{y,i}$	Joint constraint force in y direction on link i from link $i+1$.	$h_y \in \mathbb{R}^{n-1}$
$h_{x,i-1}$	Joint constraint force in x direction on link i from link $i-1$.	$h_x \in \mathbb{R}^{n-1}$
$h_{y,i-1}$	Joint constraint force in y direction on link i from link $i-1$.	$h_y \in \mathbb{R}^{n-1}$

TABLE I
DEFINED MATHEMATICAL SYMBOLS.

$$A = \begin{bmatrix} 1 & 1 & & \\ & \ddots & \ddots & \\ & & 1 & 1 \end{bmatrix}, D = \begin{bmatrix} 1 & -1 & & \\ & \ddots & \ddots & \\ & & 1 & -1 \end{bmatrix}$$

where $A \in \mathbb{R}^{(n-1)\times n}$ and $D \in \mathbb{R}^{(n-1)\times n}$. Furthermore,

$$e = \begin{bmatrix} 1 & \cdots & 1 \end{bmatrix}^T \in \mathbb{R}^n, \quad E = \begin{bmatrix} e & 0_{n\times 1} \\ 0_{n\times 1} & e \end{bmatrix} \in \mathbb{R}^{2n\times 2},$$

$$\sin\theta = \begin{bmatrix} \sin\theta_1 \,..\, \sin\theta_n \end{bmatrix}^T \in \mathbb{R}^n, \quad S_\theta = \operatorname{diag}(\sin\theta) \in \mathbb{R}^{n\times n},$$

$$\cos\theta = \begin{bmatrix} \cos\theta_1 \,..\, \cos\theta_n \end{bmatrix}^T \in \mathbb{R}^n, \quad C_\theta = \operatorname{diag}(\cos\theta) \in \mathbb{R}^{n\times n}.$$

Note that the operator $\operatorname{diag}(\cdot)$ produces a diagonal matrix with the elements of its argument along its diagonal. Note also that $\sin(\cdot)$ and $\cos(\cdot)$ are vector operators when their argument is a vector and scalar operators when their argument is a scalar value. As shown in Table I, we will use subscript i to denote element i of a vector. When parameters of the links of the snake robot are assembled into a vector, we associate element i of this vector with link i.

B. Kinematics

The snake robot moves in the horizontal plane and has a total of $n+2$ degrees of freedom. The absolute angle, θ_i, of link i is expressed with respect to the global x axis with counterclockwise positive direction. As seen in Fig. 2, the relative angle between link i and link $i+1$ is given by $\phi_i = \theta_i - \theta_{i+1}$. The local coordinate system of each link is fixed in the CM (center of mass) of the link with x (tangential) and y (normal) axes oriented such that they are oriented in the directions of the global x and y axis, respectively, when the link angle is zero. The rotation matrix from the global frame to the frame of link i is given by

$$R_{\text{link},i}^{\text{global}} = \begin{bmatrix} \cos\theta_i & -\sin\theta_i \\ \sin\theta_i & \cos\theta_i \end{bmatrix}. \tag{10}$$

The position, p, of the CM (center of mass) of the snake robot is given by

$$p = \begin{bmatrix} p_x \\ p_y \end{bmatrix} = \begin{bmatrix} \frac{1}{nm}\sum_{i=1}^{n} m x_i \\ \frac{1}{nm}\sum_{i=1}^{n} m y_i \end{bmatrix} = \frac{1}{n}\begin{bmatrix} e^T x \\ e^T y \end{bmatrix}. \tag{11}$$

It is shown in [18] that the global frame position of the CM of each link is given by

$$\begin{aligned} x &= -lN^T \cos\theta + e p_x \\ y &= -lN^T \sin\theta + e p_y \end{aligned} \tag{12}$$

where

$$N = A^T \left(DD^T\right)^{-1} D \in \mathbb{R}^{n\times n}. \tag{13}$$

The linear velocities of the links are derived by differentiating (12). This gives

$$\begin{aligned} \dot{x} &= lN^T S_\theta \dot{\theta} + e\dot{p}_x \\ \dot{y} &= -lN^T C_\theta \dot{\theta} + e\dot{p}_y. \end{aligned} \tag{14}$$

An expression for the velocity of a single link may be found by investigating the structure of each row in (14). The derivation is not included here due to space restrictions, but it may be

verified that the linear velocity of the CM of link i in the global x and y directions is given by

$$\begin{aligned} \dot{x}_i &= \dot{p}_x - \sigma_i S_\theta \dot{\theta} \\ \dot{y}_i &= \dot{p}_y + \sigma_i C_\theta \dot{\theta} \end{aligned} \tag{15}$$

where

$$\begin{aligned} \sigma_i &= \begin{bmatrix} a_1 & a_2 & \dots & a_{i-1} & \frac{a_i+b_i}{2} & b_{i+1} & b_{i+2} & \dots & b_n \end{bmatrix} \in \mathbb{R}^n \\ a_i &= \tfrac{l(2i-1)}{n} \\ b_i &= \tfrac{l(2i-1-2n)}{n}. \end{aligned} \tag{16}$$

C. Viscous friction model

In this paper, we consider snake robots influenced by viscous ground friction forces. In this section, we present the viscous friction model, and in particular we present models for the different cases of isotropic versus anisotropic viscous friction.

1) Isotropic viscous friction: The friction forces are assumed to act on the CM of the links only. The isotropic viscous friction force on link i in the global x and y direction is proportional to the global velocity of the link and is written

$$\begin{aligned} f_{R,x,i} &= -c\dot{x}_i = -c\dot{p}_x + c\sigma_i S_\theta \dot{\theta} \\ f_{R,y,i} &= -c\dot{y}_i = -c\dot{p}_y - c\sigma_i C_\theta \dot{\theta} \end{aligned} \tag{17}$$

where c is the viscous friction coefficient, and the expression for the link velocity is given by (15). The friction forces on all links may be expressed in matrix form as

$$f_R = \begin{bmatrix} f_{R,x} \\ f_{R,y} \end{bmatrix} = -c \begin{bmatrix} \dot{x} \\ \dot{y} \end{bmatrix} = -c \begin{bmatrix} lN^T S_\theta \dot{\theta} + e\dot{p}_x \\ -lN^T C_\theta \dot{\theta} + e\dot{p}_y \end{bmatrix} \tag{18}$$

where the expression for the link velocities is given by (14). We disregard the friction torque caused by a link rotating with respect to the ground since this torque only has a minor impact on the motion.

2) Anisotropic viscous friction: Under anisotropic friction conditions, a link has two viscous friction coefficients, c_t and c_n, describing the friction force in the tangential (along link x axis) and normal (along link y axis) direction of the link, respectively. Using (10), the friction force on link i in the global frame as a function of the global link velocity, $\dot{x}_i$ and $\dot{y}_i$, is given by

$$\begin{aligned} f_{R,i}^{\text{global}} &= R_{\text{link},i}^{\text{global}} f_{R,i}^{\text{link},i} = -R_{\text{link},i}^{\text{global}} \begin{bmatrix} c_t & 0 \\ 0 & c_n \end{bmatrix} v_i^{\text{link},i} \\ &= -R_{\text{link},i}^{\text{global}} \begin{bmatrix} c_t & 0 \\ 0 & c_n \end{bmatrix} \left(R_{\text{link},i}^{\text{global}} \right)^T \begin{bmatrix} \dot{x}_i \\ \dot{y}_i \end{bmatrix} \end{aligned} \tag{19}$$

where $f_{R,i}^{\text{link},i}$ and $v_i^{\text{link},i}$ are, respectively, the friction force and the link velocity expressed in the local link frame. Performing the matrix multiplication and assembling the friction forces on all links in matrix form gives

$$f_R = -\begin{bmatrix} c_t \left(C_\theta\right)^2 + c_n \left(S_\theta\right)^2 & \left(c_t - c_n\right) S_\theta C_\theta \\ \left(c_t - c_n\right) S_\theta C_\theta & c_t \left(S_\theta\right)^2 + c_n \left(C_\theta\right)^2 \end{bmatrix} \begin{bmatrix} \dot{x} \\ \dot{y} \end{bmatrix} \tag{20}$$

where $f_R = \begin{bmatrix} f_{R,x}^T & f_{R,y}^T \end{bmatrix}^T \in \mathbb{R}^{2n}$. Note that (20) reduces to (18) in the case of isotropic friction ($c_t = c_n = c$).

D. Equations of motion

This section presents the equations of motion of the snake robot in terms of the acceleration of the link angles, $\ddot{\theta}$, and the acceleration of the CM of the snake robot, $\ddot{p}$. These coordinates describe all $n+2$ DOFs of the snake robot.

The forces and torques acting on link i are visualized in Fig. 3. The force balance for link i in global frame coordinates is given by

$$\begin{aligned} m\ddot{x}_i &= f_{R,x,i} + h_{x,i} - h_{x,i-1} \\ m\ddot{y}_i &= f_{R,y,i} + h_{y,i} - h_{y,i-1} \end{aligned} \tag{21}$$

while the torque balance for link i is given by

$$\begin{aligned} J\ddot{\theta}_i &= u_i - u_{i-1} \\ -l\sin\theta_i (h_{x,i} + h_{x,i-1}) + l\cos\theta_i (h_{y,i} + h_{y,i-1}). \end{aligned} \tag{22}$$

Through straightforward calculations, it is shown in [18] that (21) and (22) may be rewritten for all links and combined into the following complete model of the snake robot:

$$M\ddot{\theta} + W\dot{\theta}^2 - lS_\theta N f_{R,x} + lC_\theta N f_{R,y} = D^T u \tag{23}$$

$$nm\ddot{p} = nm \begin{bmatrix} \ddot{p}_x \\ \ddot{p}_y \end{bmatrix} = E^T f_R = \begin{bmatrix} e^T f_{R,x} \\ e^T f_{R,y} \end{bmatrix} \tag{24}$$

where θ and p represent the $n+2$ generalized coordinates of the system, $\dot{\theta}^2 = \text{diag}(\dot{\theta})\dot{\theta}$, and

$$\begin{aligned} M &= JI_{n\times n} + ml^2 \left(S_\theta V S_\theta + C_\theta V C_\theta\right) \\ W &= ml^2 \left(S_\theta V C_\theta - C_\theta V S_\theta\right) \\ N &= A^T \left(DD^T\right)^{-1} D \\ V &= A^T \left(DD^T\right)^{-1} A. \end{aligned} \tag{25}$$

The model of the snake robot may be written more compactly as

$$\dot{x} = \begin{bmatrix} \dot{\theta}^T & \dot{p}^T & \ddot{\theta}^T & \ddot{p}^T \end{bmatrix}^T = F(x,t) \tag{26}$$

where we have introduced the state variable $x = \begin{bmatrix} \theta^T & p^T & \dot{\theta}^T & \dot{p}^T \end{bmatrix}^T \in \mathbb{R}^{2n+4}$ and also assumed that $u = u(x,t)$. The elements of $F(x,t)$ are given by solving (23) and (24) for $\ddot{\theta}$ and $\ddot{p}$, respectively.

V. Partial feedback linearization of the model

This section transforms the model (26) to a simpler form through partial feedback linearization [24], [25]. This conversion greatly simplifies the controllability analysis presented in Section VII. Partial feedback linearization of underactuated systems consists of linearizing the dynamics corresponding to the actuated degrees of freedom of the system. In this section, we show how a change of coordinates makes it possible to employ this methodology by following the approach presented in [26].

A. Partitioning the model into an actuated and an unactuated part

Before partial feedback linearization can be carried out, the model of the snake robot in (26) must be partitioned into two parts representing the actuated and unactuated degrees of freedom, respectively [26]. The acceleration of the CM of the snake robot, $\ddot{p}$, belongs to the unactuated part since it is not directly influenced by the input, u. The acceleration

of the link angles, $\ddot{\theta}$, represents one unactuated degree of freedom and $n-1$ actuated degrees of freedom since there are n link accelerations ($\theta \in \mathbb{R}^n$) and only $n-1$ control inputs ($u \in \mathbb{R}^{n-1}$). However, it is not possible to partition the equation for $\ddot{\theta}$ in (23) into an actuated and an unactuated part since the matrix D^T in front of the control input gives a direct influence between u and all the link accelerations. We therefore seek a form of the model where there is a direct influence between u and only $n-1$ link accelerations. This is achieved by modifying the choice of generalized coordinates from absolute link angles to relative joint angles. The generalized coordinates of the model in (26) are given by the absolute link angles, θ, and the CM position of the snake robot, p. We now replace these coordinates with

$$q = \begin{bmatrix} \phi \\ p \end{bmatrix} \in \mathbb{R}^{n+2} \tag{27}$$

where

$$\phi = \begin{bmatrix} \phi_1 & \phi_2 & \cdots & \phi_{n-1} & \theta_n \end{bmatrix}^T \in \mathbb{R}^n \tag{28}$$

contains the $n-1$ relative joint angles of the snake robot and the absolute link angle, $\theta_n \in \mathbb{R}$, of the head link. The relative joint angles are defined in Fig. 2. The coordinate transformation between absolute link angles and relative joint angles is easily shown to be given by

$$\theta = R\phi \tag{29}$$

$$R = \begin{bmatrix} 1 & 1 & 1 & \cdots & 1 & 1 \\ 0 & 1 & 1 & \cdots & 1 & 1 \\ \vdots & & & & & \vdots \\ 0 & 0 & 0 & \cdots & 0 & 1 \end{bmatrix} \in \mathbb{R}^{n \times n}. \tag{30}$$

The dynamic model in the new coordinates is found by inserting (29) into (23) and (24). This gives

$$\begin{array}{c} MR\ddot{\phi} + W \operatorname{diag}\left(R\dot{\phi}\right) R\dot{\phi} - lS_\theta N f_{R,x} \\ +lC_\theta N f_{R,y} = D^T u \\ nm\ddot{p} = E^T f_R \end{array} \tag{31}$$

where we have used that $\dot{\theta}^2 = \operatorname{diag}(\dot{\theta})\dot{\theta} = \operatorname{diag}\left(R\dot{\phi}\right) R\dot{\phi}$. Finally, we premultiply the first matrix equation in (31) with R^T in order to achieve the desired form of the input mapping matrix on the right-hand side by making the last of the n equations independent of the control input. This enables us to write the complete model of the snake robot as

$$\overline{M}(\phi)\ddot{q} + \overline{W}\left(\phi, \dot{\phi}\right) + \overline{G}(\phi) f_R\left(\phi, \dot{\phi}, \dot{p}\right) = \overline{B}u \tag{32}$$

where

$$q = \begin{bmatrix} \phi \\ p \end{bmatrix} \in \mathbb{R}^{n+2} \tag{33}$$

$$\overline{M}(\phi) = \begin{bmatrix} R^T M(\phi) R & 0_{n\times 2} \\ 0_{2\times n} & nmI_2 \end{bmatrix} \tag{34}$$

$$\overline{W}\left(\phi, \dot{\phi}\right) = \begin{bmatrix} R^T W(\phi) \operatorname{diag}\left(R\dot{\phi}\right) R\dot{\phi} \\ 0_{2\times 1} \end{bmatrix} \tag{35}$$

$$\overline{G}(\phi) = \begin{bmatrix} -lR^T S_{R\phi} N & lR^T C_{R\phi} N \\ -e^T & 0_{1\times n} \\ 0_{1\times n} & -e^T \end{bmatrix} \tag{36}$$

$$\overline{B} = \begin{bmatrix} I_{n-1} \\ 0_{3\times n-1} \end{bmatrix} \tag{37}$$

and where $S_{R\phi} = S_\theta$ and $C_{R\phi} = C_\theta$. It is interesting to note that premultiplying the first matrix equation in (31) with R^T both causes the input mapping matrix to attain a desirable form and produces a symmetrical inertia matrix. Had we left the model in the form of (31), the inertia matrix would not have been symmetrical.

The first $n-1$ equations of (32) represent the dynamics of the relative joint angles of the snake robot, i.e. the *actuated* degrees of freedom of the snake robot. The last three equations represent the dynamics of the absolute orientation and position of the snake robot, i.e. the *unactuated* degrees of freedom. The model may therefore be partitioned as

$$\overline{M}_{11}\ddot{q}_a + \overline{M}_{12}\ddot{q}_u + \overline{W}_1 + \overline{G}_1 f_R = u \tag{38}$$

$$\overline{M}_{21}\ddot{q}_a + \overline{M}_{22}\ddot{q}_u + \overline{W}_2 + \overline{G}_2 f_R = 0_{3\times 1} \tag{39}$$

where $q_a = \begin{bmatrix} \phi_1 & \cdots & \phi_{n-1} \end{bmatrix}^T \in \mathbb{R}^{n-1}$ represents the actuated degrees of freedom, $q_u = \begin{bmatrix} \theta_n & p_x & p_y \end{bmatrix}^T \in \mathbb{R}^3$ represents the unactuated degrees of freedom, $\overline{M}_{11} \in \mathbb{R}^{(n-1)\times(n-1)}$, $\overline{M}_{12} \in \mathbb{R}^{(n-1)\times 3}$, $\overline{M}_{21} \in \mathbb{R}^{3\times(n-1)}$, $\overline{M}_{22} \in \mathbb{R}^{3\times 3}$, $\overline{W}_1 \in \mathbb{R}^{n-1}$, $\overline{W}_2 \in \mathbb{R}^3$, $\overline{G}_1 \in \mathbb{R}^{(n-1)\times 2n}$, and $\overline{G}_2 \in \mathbb{R}^{3\times 2n}$. Note that $\overline{M}(\phi)$ only depends on the relative joint angles of the snake robot and not on the absolute orientation of the head link, θ_n. Formally, this is a result of the fact that θ_n is a *cyclic* coordinate [27]. Less formally, this is quite obvious since it would not be reasonable that the inertial properties of a planar snake robot be dependent on how the snake robot is oriented in the plane. We therefore have that $\overline{M} = \overline{M}(q_a)$.

B. Partial feedback linearization

We are now ready to present an input transformation that linearizes the dynamics of the actuated degrees of freedom in (38). $\overline{M}_{22}$ is an invertible 3×3 matrix as a consequence of the uniform positive definiteness of the complete system inertia matrix, $\overline{M}(q_a)$. We may therefore solve (39) for $\ddot{q}_u$ as

$$\ddot{q}_u = -\overline{M}_{22}^{-1}\left(\overline{M}_{21}\ddot{q}_a + \overline{W}_2 + \overline{G}_2 f_R\right). \tag{40}$$

Inserting (40) into (38) gives

$$\begin{array}{c} \left(\overline{M}_{11} - \overline{M}_{12}\overline{M}_{22}^{-1}\overline{M}_{21}\right)\ddot{q}_a + \overline{W}_1 + \overline{G}_1 f_R \\ -\overline{M}_{12}\overline{M}_{22}^{-1}\left(\overline{W}_2 + \overline{G}_2 f_R\right) = u. \end{array} \tag{41}$$

Consequently, the following linearizing controller

$$u = \left(\overline{M}_{11} - \overline{M}_{12}\overline{M}_{22}^{-1}\overline{M}_{21}\right) v + \overline{W}_1 + \overline{G}_1 f_R - \overline{M}_{12}\overline{M}_{22}^{-1}\left(\overline{W}_2 + \overline{G}_2 f_R\right) \tag{42}$$

enables us to rewrite (38) and (39) as

$$\ddot{q}_a = v \tag{43}$$

$$\ddot{q}_u = \mathcal{A}(q, \dot{q}) + \mathcal{B}(q_a)\, v \tag{44}$$

where

$$\mathcal{A}(q, \dot{q}) = -\overline{M}_{22}^{-1}\left(\overline{W}_2 + \overline{G}_2 f_R\right) \in \mathbb{R}^3 \tag{45}$$

$$\mathcal{B}(q_a) = -\overline{M}_{22}^{-1}\overline{M}_{21} \in \mathbb{R}^{3\times(n-1)}. \tag{46}$$

This model may be written in the standard form of a control-affine system by defining $x_1 = q_a$, $x_2 = q_u$, $x_3 = \dot{q}_a$, $x_4 = \dot{q}_u$, and $x = \begin{bmatrix} x_1^T & x_2^T & x_3^T & x_4^T \end{bmatrix}^T \in \mathbb{R}^{2n+4}$. This gives

$$\dot{x} = \begin{bmatrix} \dot{x}_1 \\ \dot{x}_2 \\ \dot{x}_3 \\ \dot{x}_4 \end{bmatrix} = \begin{bmatrix} x_3 \\ x_4 \\ v \\ \mathcal{A}(x) + \mathcal{B}(x_1)\, v \end{bmatrix} = f(x) + \sum_{j=1}^{n-1} g_j(x_1)\, v_j \tag{47}$$

where

$$f(x) = \begin{bmatrix} x_3 \\ x_4 \\ 0_{(n-1)\times 1} \\ \mathcal{A}(x) \end{bmatrix}, g_j(x_1) = \begin{bmatrix} 0_{(n-1)\times 1} \\ 0_{3\times 1} \\ e_j \\ \mathcal{B}_j(x_1) \end{bmatrix} \tag{48}$$

and where e_j denotes the jth standard basis vector in $\mathbb{R}^{n-1}$ (the jth column of I_{n-1}), and $\mathcal{B}_j(x_1)$ denotes the jth column of $\mathcal{B}(x_1)$.

VI. Stabilizability properties of planar snake robots

This section presents a fundamental theorem concerning the properties of an asymptotically stabilizing control law for snake robots to any equilibrium point. The equation (47) maps the state, x, and the controller input, v, of the robot into the resulting derivative of the state vector, $\dot{x}$. For any equilibrium point $(x_1 = x_1^e, x_2 = x_2^e, x_3 = 0, x_4 = 0)$, where (x_1^e, x_2^e) is the configuration of the system at the equilibrium point, we have that $\dot{x} = 0$.

A well-known result by Brockett [28] states that a necessary condition for the existence of a *time-invariant* (i.e. not explicitly dependent on time) *continuous* state feedback law, $v = v(x)$, that makes $(x_1^e, x_2^e, 0, 0)$ asymptotically stable, is that the image of the mapping $(x, v) \mapsto \dot{x}$ contains some neighbourhood of $\dot{x} = 0$. A result by Coron and Rosier [29] states that a control system that can be asymptotically stabilized (in the Filippov sense [29]) by a *time-invariant discontinuous* state feedback law can be asymptotically stabilized by a *continuous time-varying* state feedback law. If, moreover, the control system is *affine* (i.e. linear with respect to the control input), then it can be asymptotically stabilized by a *time-invariant continuous* state feedback law. We now employ these results to prove the following fundamental theorem for planar snake robots:

Theorem 3: An asymptotically stabilizing control law for a planar snake robot described by (47) to any equilibrium point must be time-varying, i.e. of the form $v = v(x, t)$.

Proof: The result by Brockett [28] states that the mapping $(x_1, x_2, x_3, x_4, v) \mapsto (x_3, x_4, v, \mathcal{A}(x) + \mathcal{B}(x_1)\, v)$ must map an arbitrary neighbourhood of $(x_1 = x_1^e, x_2 = x_2^e, x_3 = 0, x_4 = 0, v = 0)$ onto a neighbourhood of $(x_3 = 0, x_4 = 0, v = 0, \mathcal{A}(x) + \mathcal{B}(x_1)\, v = 0)$. For this to be true, points of the form $(x_3 = 0, x_4 = 0, v = 0, \mathcal{A}(x) + \mathcal{B}(x_1)\, v = \epsilon)$ must be contained in this mapping for some arbitrary $\epsilon \neq 0$ because points of this form are contained in every neighbourhood of $\dot{x} = 0$. However, these points do not exist for the system in (47) because $x_3 = 0$, $x_4 = 0$, and $v = 0$ means that $\mathcal{A}(x) + \mathcal{B}(x_1)\, v = 0 \neq \epsilon$. Hence, the snake robot *cannot* be asymptotically stabilized to $(x_1 = x_1^e, x_2 = x_2^e, x_3 = 0, x_4 = 0)$ by a *time-invariant continuous* state feedback law. Moreover, since the system in (47) is affine and *cannot* be asymptotically stabilized by a *time-invariant continuous* state feedback law, the result by Coron and Rosier [29] proves that the system can neither be asymptotically stabilized by a *time-invariant discontinuous* state feedback law. We can therefore conclude that an asymptotically stabilizing control law for a planar snake robot to any equilibrium point must be time-varying, i.e. of the form $v = v(x, t)$. ∎

Remark 4: Theorem 3 is independent of the choice of friction model and applies to any planar snake robot described by a friction model with the property that $\mathcal{A}(x^e) = 0$ for any equilibrium point x^e.

VII. Controllability analysis of planar snake robots

This section studies the controllability of planar snake robots influenced by viscous ground friction.

A. Controllability with isotropic viscous friction

We begin the controllability analysis of the snake robot by first assuming that the viscous ground friction is isotropic. In this case, it turns out that the equations of motion take on a particularly simple form that enables us to study controllability through pure inspection of the equations of motion. From (24), we have that the acceleration of the CM (center of mass) of the snake robot is given by

$$\begin{bmatrix} \ddot{p}_x \\ \ddot{p}_y \end{bmatrix} = \begin{bmatrix} \frac{1}{nm} e^T f_{R,x} \\ \frac{1}{nm} e^T f_{R,y} \end{bmatrix} = \frac{1}{nm} \begin{bmatrix} \sum_{i=1}^{n} f_{R,x,i} \\ \sum_{i=1}^{n} f_{R,y,i} \end{bmatrix}. \tag{49}$$

Inserting (17) into (49) gives

$$\begin{bmatrix} \ddot{p}_x \\ \ddot{p}_y \end{bmatrix} = \frac{c}{nm} \begin{bmatrix} -n\dot{p}_x + \left(\sum_{i=1}^{n} \sigma_i\right) S_\theta \dot{\theta} \\ -n\dot{p}_y - \left(\sum_{i=1}^{n} \sigma_i\right) C_\theta \dot{\theta} \end{bmatrix} = -\frac{c}{m} \begin{bmatrix} \dot{p}_x \\ \dot{p}_y \end{bmatrix} \tag{50}$$

because it may be shown that $\sum_{i=1}^{n}\sigma_i = 0$. This enables us to state the following theorem:

Theorem 5: A planar snake robot influenced by *isotropic* viscous ground friction is *not controllable*.

Proof: In order to control the position, the snake robot must accelerate its CM (center of mass). From (50) it is clear that the CM acceleration is proportional to the CM velocity. If the snake robot starts from rest ($\dot{p} = 0$), it is therefore impossible to achieve acceleration of the CM. The position of the snake robot is in other words completely uncontrollable in this case, which renders the snake robot uncontrollable. ■

B. Controllability with anisotropic viscous friction

The equations of motion of the snake robot in (47) become far more complex under anisotropic friction conditions. We therefore employ the controllability concepts presented in Section II and begin by computing the Lie brackets of the system vector fields. The drift and control vector fields of the snake robot are given in (48). As explained in Section II, Lie bracket computation involves partial derivatives of the components of the vector fields. These computations can be carried out without dealing with the complex expressions contained in $\mathcal{A}(x)$ and $\mathcal{B}(x_1)$ given by (45) and (46), respectively, since we only need to know which variables each row of the vector fields depend on. As an example, consider column j of $\mathcal{B}(x_1)$. Since we know that it only depends on x_1, we may immediately write $\frac{\partial \mathcal{B}_j(x_1)}{\partial x} = \begin{bmatrix}\frac{\partial \mathcal{B}_j(x_1)}{\partial x_1} & 0_{3\times(n+5)}\end{bmatrix}$. This methodology enables us to compute the following Lie brackets of the system vector fields (evaluated at an equilibrium point):

$$[f,g_j]^{\dot{q}=0} = \begin{bmatrix} -e_j \\ -\mathcal{B}_j \\ 0_{(n-1)\times 1} \\ -\mathcal{C}_j \end{bmatrix}, [f,[f,g_j]]^{\dot{q}=0} = \begin{bmatrix} 0_{(n-1)\times 1} \\ \mathcal{C}_j \\ 0_{(n-1)\times 1} \\ \frac{\partial \mathcal{A}}{\partial x_4}\mathcal{C}_j \end{bmatrix},$$
$$[[f,g_j],[f,g_k]]^{\dot{q}=0} = \begin{bmatrix} 0_{(n-1)\times 1} \\ \mathcal{D}_{jk} \\ 0_{(n-1)\times 1} \\ \mathcal{E}_{jk} \end{bmatrix} \tag{51}$$

where $j,k \in \{1,...,n-1\}$ and

$$\mathcal{C}_j = \frac{\partial \mathcal{A}}{\partial x_3}e_j + \frac{\partial \mathcal{A}}{\partial x_4}\mathcal{B}_j \ , \ \mathcal{D}_{jk} = \frac{\partial \mathcal{B}_k}{\partial x_1}e_j - \frac{\partial \mathcal{B}_j}{\partial x_1}e_k,$$
$$\mathcal{E}_{jk} = \frac{\partial \mathcal{C}_k}{\partial x_1}e_j - \frac{\partial \mathcal{C}_j}{\partial x_1}e_k + \frac{\partial \mathcal{C}_k}{\partial x_2}\mathcal{B}_j - \frac{\partial \mathcal{C}_j}{\partial x_2}\mathcal{B}_k + \frac{\partial \mathcal{C}_k}{\partial x_4}\mathcal{C}_j - \frac{\partial \mathcal{C}_j}{\partial x_4}\mathcal{C}_k. \tag{52}$$

The Lie brackets have been evaluated at zero velocity ($\dot{q} = 0$) since we are interested in controllability from an equilibrium point. The above vector fields represent our choice of vector fields to be contained in the *accessibility algebra*, Δ, of the system. To construct Δ of full rank, we need to find $(2n+4)$ independent vector fields since the snake robot has a $(2n+4)$-dimensional state space. Each of the four types of vector fields above represent $(n-1)$ vector fields. Solving $4(n-1) \geq 2n+4$ gives that our analysis is only valid if the snake robot has $n \geq 4$ links. This is a mild requirement, however, since a snake robot generally will have more than four links. In the remainder of this section, we assume that the robot consists of exactly $n = 4$ links (and thereby $n-1 = 3$ active joints) and argue that the following controllability results will also be valid for snake robots with more links. In particular, a robot with $n > 4$ links can behave as a robot with $n = 4$ links by fixing $(n-4)$ joint angles at zero degrees and allowing the remaining three joint angles to move. This means that controllability of the robot with $n = 4$ is a sufficient although not necessary condition for controllability with $n > 4$.

With $n = 4$ links, the system has a $(2n+4) = 12$-dimensional state space. The system satisfies the *Lie algebra rank condition* (LARC) if the above vector fields span a 12-dimensional space. We therefore assemble the 12 vector fields into the following matrix, which represents the *accessibility algebra* of the system evaluated at an equilibrium point x^e:

$$\begin{aligned}\Delta(x^e) &= [g_1,g_2,g_3,[f,g_1],[f,g_2],[f,g_3], \\ &\quad [f,[f,g_1]],[f,[f,g_2]],[f,[f,g_3]], \\ &\quad [[f,g_1],[f,g_2]],[[f,g_1],[f,g_3]],[[f,g_2],[f,g_3]]] \\ &= \begin{bmatrix} 0_{3\times 3} & -I_3 & 0_{3\times 3} & 0_{3\times 3} \\ 0_{3\times 3} & -\mathcal{B} & \mathcal{C} & \mathcal{D} \\ I_3 & 0_{3\times 3} & 0_{3\times 3} & 0_{3\times 3} \\ \mathcal{B} & -\mathcal{C} & \frac{\partial \mathcal{A}}{\partial x_4}\mathcal{C} & \mathcal{E} \end{bmatrix} \in \mathbb{R}^{12\times 12}\end{aligned} \tag{53}$$

where

$$\mathcal{C} = \frac{\partial \mathcal{A}}{\partial x_3} + \frac{\partial \mathcal{A}}{\partial x_4}\mathcal{B} \in \mathbb{R}^{3\times 3},$$
$$\mathcal{D} = \begin{bmatrix}\mathcal{D}_{12} & \mathcal{D}_{13} & \mathcal{D}_{23}\end{bmatrix}, \mathcal{E} = \begin{bmatrix}\mathcal{E}_{12} & \mathcal{E}_{13} & \mathcal{E}_{23}\end{bmatrix}. \tag{54}$$

We now state the following theorem regarding the accessibility of the snake robot:

Theorem 6: A planar snake robot with $n \geq 4$ links influenced by *anisotropic* viscous ground friction ($c_t \neq c_n$) is *locally strongly accessible* from any equilibrium point x^e ($\dot{q} = 0$) satisfying $\det(\mathcal{C}) \neq 0$ and $\det\left(\mathcal{E} - \frac{\partial \mathcal{A}}{\partial x_4}\mathcal{D}\right) \neq 0$, where $\det(*)$ denotes the determinant evaluated at x^e.

Proof: By Theorem 1, the system is *locally strongly accessible* from x^e if $\Delta(x^e)$, given by (53), has full rank, i.e. spans a 12-dimensional space. The proof is complete if we can show that this is the case as long as $\det(\mathcal{C}) \neq 0$ and $\det\left(\mathcal{E} - \frac{\partial \mathcal{A}}{\partial x_4}\mathcal{D}\right) \neq 0$ at x^e. The matrix $\Delta(x^e)$ has full rank when all its columns are linearly independent. By investigating the particular structure of $\Delta(x^e)$, we see that the first and third row contains an identity matrix and then zeros in the remaining elements of these rows. It is therefore impossible to write the columns containing the two identity matrices as linear combinations of other columns. We can therefore conclude that any linear dependence between the columns of $\Delta(x^e)$ must be caused by linear dependence between the columns of the following submatrix of $\Delta(x^e)$:

$$\widetilde{\Delta}(x^e) = \begin{bmatrix} \mathcal{C} & \mathcal{D} \\ \frac{\partial \mathcal{A}}{\partial x_4}\mathcal{C} & \mathcal{E} \end{bmatrix} \in \mathbb{R}^{6\times 6}. \tag{55}$$

Linear dependence between columns of a square matrix causes its determinant to become zero. We therefore calculate the determinant of $\widetilde{\Delta}(x^e)$ by employing the following well-known mathematical relationship concerning the determinant of a block matrix (see e.g. [30]):

$$\det\left(\begin{bmatrix} A & B \\ C & D \end{bmatrix}\right) = \det(A)\det\left(D - CA^{-1}B\right) \tag{56}$$

where A and D are any square matrices and A is non-singular. This gives

$$\det\left(\widetilde{\Delta}\left(x^e\right)\right) = \det\left(\mathcal{C}\right)\det\left(\mathcal{E}-\frac{\partial\mathcal{A}}{\partial x_4}\mathcal{D}\right). \tag{57}$$

The determinant of $\widetilde{\Delta}\left(x^e\right)$ is zero when $\det\left(\mathcal{C}\right) = 0$ or when $\det\left(\mathcal{E}-\frac{\partial\mathcal{A}}{\partial x_4}\mathcal{D}\right) = 0$. This means that $\widetilde{\Delta}\left(x^e\right)$, and thereby also $\Delta\left(x^e\right)$, has full rank whenever $\det\left(\mathcal{C}\right) \neq 0$ and $\det\left(\mathcal{E}-\frac{\partial\mathcal{A}}{\partial x_4}\mathcal{D}\right) \neq 0$. This completes the proof. ■

The requirement regarding the two determinants in Theorem 6 is not very restrictive, but it implies that the snake robot can attain configurations that are singular, i.e. certain shapes of the snake robot are obstructive from a control perspective since the dimension of the reachable space from these configurations is not full-dimensional. These singular configurations are revealed by the following property:

Property 7: The accessibility algebra $\Delta\left(x^e\right)$ of the system drops rank at equilibrium points where all relative joint angles are equal $(\phi_1 = \phi_2 = ... = \phi_{n-1})$.

This property can be shown to hold with a mathematical software tool such as *Matlab Symbolic Math Toolbox* since it can be verified that $\det\left(\mathcal{C}\right)\big|_{\phi_1=\phi_2=...=\phi_{n-1}} = 0$, thereby violating the full rank conditions that are stated in Theorem 6. Property 7 is interesting since it implies that the joint angles of a snake robot should be *out of phase* during snake locomotion. This claim has been stated in several previous works [1], [2], [8], [31], but no formal mathematical proof was given.

We now show that the snake robot does *not* satisfy sufficient conditions for *small-time local controllability* (STLC).

Theorem 8: At any equilibrium point x^e $(\dot{q} = 0)$, a planar snake robot with $n \geq 4$ links influenced by viscous ground friction does *not* satisfy the sufficient conditions for *small-time local controllability* (STLC) stated in Theorem 2.

Proof: The proof is complete if we can show that there are *bad* brackets of the system vector fields that cannot be neither *θ-neutralized* nor *l-neutralized* (see Theorem 2). The *bad* brackets with the lowest θ-degree and the lowest l-degree (except for f, which vanishes at any equilibrium point) are $[g_j, [f, g_j]]$, $j \in \{1, 2, 3\}$. Theorem 2 requires these vectors to be written as linear combinations of *good* brackets with either lower θ-degree or lower l-degree. The only such *good* brackets are $g_j, [f, g_j], [f, [f, g_j]], .., [f, [\cdots [f, g_j]] \cdots]$, $j \in \{1, 2, 3\}$. Brackets of the form $[g_k, g_j]$ are not considered because $[g_k, g_j] = 0$, $j, k \in \{1, 2, 3\}$. For a proper choice of θ and l_j, $j \in \{0, 1, 2, 3\}$, these brackets have both lower θ-degree and lower l-degree. It is straightforward to verify that $[g_j, [f, g_j]] \in \mathbb{R}^{2n+4=12}$ is a vector of all zeros except for element number $2n + 2 = 10$. The only way to write this vector as a linear combination of the *good* brackets listed above is if these *good* brackets span the entire 12-dimensional state space. This is not the case, however, because the vectors $[f, [f, g_j]], .., [f, [\cdots [f, g_j]] \cdots]$ are linearly dependent, as can be seen by assembling the following matrix:

$$\begin{aligned}&\left[[f, [f, g_j]], [f, [f, [f, g_j]]], [f, [f, [f, [f, g_j]]]], \cdots\right]\\ &= \begin{bmatrix} 0_{3\times3} & 0_{3\times3} & 0_{3\times3} & \cdots \\ \mathcal{C} & -\frac{\partial\mathcal{A}}{\partial x_4}\mathcal{C} & \left(\frac{\partial\mathcal{A}}{\partial x_4}\right)^2\mathcal{C} & \cdots \\ 0_{3\times3} & 0_{3\times3} & 0_{3\times3} & \cdots \\ \frac{\partial\mathcal{A}}{\partial x_4}\mathcal{C} & -\left(\frac{\partial\mathcal{A}}{\partial x_4}\right)^2\mathcal{C} & \left(\frac{\partial\mathcal{A}}{\partial x_4}\right)^3\mathcal{C} & \cdots \end{bmatrix}\end{aligned} \tag{58}$$

and noting that the fourth row is a multiple of the second row. It is therefore not possible to either *θ-neutralize* nor *l-neutralize* the *bad* brackets of the system in (47). The linear dependence in (58) is also present for $n > 4$ links since the six non-zero rows of (58) concern the position and head angle of the snake while the $2n - 2$ remaining rows will be zero regardless of n. This completes the proof. ■

Note that Theorem 8 does not claim that the snake robot is not STLC. In other words, the snake robot may be STLC even though the sufficient conditions of Theorem 2 are violated. Note also that STLC is not a requirement for controllability since, as described in Section II, it is in fact a stronger property than controllability. In summary, the above results do not enable us to conclude that a wheelless snake robot influenced by anisotropic ground friction is controllable. However, the above results are hopefully an important step towards formally proving that such mechanisms are controllable, which the authors consider highly likely to be the case.

We end this section with a note on Theorem 6. This theorem clearly shows that *anisotropic* friction is an important property for a snake robot. In the snake robot literature, it is common for snake robots to possess the property $c_n \gg c_t$. The extreme case of this property is realized by installing passive wheels along the snake body since this ideally means that $c_t = 0$ and $c_n = \infty$. However, from Theorem 6 it is clear that the only requirement for *strong accessibility* is that the friction coefficients are *not equal*. The property $c_t > c_n$ is therefore also valid. This means that the passive wheels commonly mounted tangential to the snake body may equally well be mounted transversal to the snake body. The resulting motion will of course be different, but the *strong accessibility* property is still preserved.

VIII. Explanation and Synthesis of Snake Locomotion

This section presents an analysis of snake locomotion that explains how anisotropic viscous ground friction enables snake robots to locomote forward on a planar surface. The analysis is subsequently used to synthesise how the snake robot links should be moved in order to propel the snake robot forward.

A. Analysis of propulsive forces during snake locomotion

Anisotropic friction generally means that the friction coefficients in the tangential and normal direction of the links are different ($c_t \neq c_n$). However, we will only focus on the commonly assumed property of snake robots that the normal direction friction is larger than the tangential friction ($c_t < c_n$).

We first derive an expression for the total force propelling the CM (center of mass) of the snake robot forward as a

function of the linear link velocities. We will call this the *propulsive force* on the snake robot and denote it by F_{prop}. The forward direction of motion is assumed to be along the global positive x axis. As described in Section IV-B, the angle θ_i of link i is expressed with respect to the global x axis with counterclockwise positive direction. The *propulsive force* is simply the sum of all external forces on the snake robot in the global x direction and is given from (24) as

$$F_{\text{prop}} = nm\ddot{p}_x = e^T f_{R,x}. \tag{59}$$

Inserting $f_{R,x}$ from (20) into (59) gives

$$F_{\text{prop}} = -e^T\Big(\big(c_t(C_\theta)^2 + c_n(S_\theta)^2\big)\dot{x} + (c_t - c_n)S_\theta C_\theta \dot{y}\Big). \tag{60}$$

The purpose of the vector e^T is to sum up the friction force contributions from all the links. We may therefore write (60) as a summation in order to investigate the force contribution from a single link.

$$\begin{aligned} F_{\text{prop}} = -\textstyle\sum_{i=1}^{n} \big(&\big(c_t \cos^2\theta_i + c_n \sin^2\theta_i\big)\dot{x}_i \\ &+ (c_t - c_n)\sin\theta_i \cos\theta_i \dot{y}_i\big). \end{aligned} \tag{61}$$

The *propulsive force* from a single link, $F_{\text{prop},i}$, is in other words given by

$$F_{\text{prop},i} = -F_x(\theta_i)\,\dot{x}_i - F_y(\theta_i)\,\dot{y}_i \tag{62}$$

where

$$\begin{aligned} F_x(\theta_i) &= c_t \cos^2\theta_i + c_n \sin^2\theta_i \\ F_y(\theta_i) &= (c_t - c_n)\sin\theta_i \cos\theta_i. \end{aligned} \tag{63}$$

We see from (62) that $F_{\text{prop},i}$ consists of two components, i.e. one involving the linear velocity of the link in the *forward* direction of motion, $F_x(\theta_i)\,\dot{x}_i$, and one involving the linear velocity *normal* to the direction of motion, $F_y(\theta_i)\,\dot{y}_i$. Due to the minus signs in (62), the products $F_x(\theta_i)\,\dot{x}_i$ and $F_y(\theta_i)\,\dot{y}_i$ provide a positive contribution to the propulsive force only if they are *negative*. Since the viscous friction coefficients, c_t and c_n, are always positive, the expression $F_x(\theta_i)$ is obviously always positive. We assume that the snake robot is not generating waves that involve x direction velocities of any of the links opposite to the direction of motion. When the snake robot is moving in the forward direction ($\dot{p}_x > 0$), we therefore have that $\dot{x}_i > 0$, which means that the product $F_x(\theta_i)\,\dot{x}_i$ of the propulsive force is always positive. This product is therefore *not* contributing to the forward propulsion of the robot, but rather opposing it. This is also expected since the snake robot must naturally be subjected to a friction force in the opposite direction of the motion.

Any maintained propulsive force in the forward direction of motion must therefore be produced by the sideways motion of the links, i.e. the product $F_y(\theta_i)\,\dot{y}_i$. A plot of $F_y(\theta_i)$ for different values of the normal friction coefficient c_n, while keeping the tangential friction coefficient c_t fixed, is shown in Fig. 4. For each plot, the angle between the link and the forward direction, θ_i, is varied from $-90°$ to $90°$.

The sideways motion of the links have no effect on the propulsive force on the snake robot when the friction coefficients are equal since this gives $F_y(\theta_i) = 0$. However, when $c_n > c_t$, Fig. (4) reveals that $F_y(\theta_i)$ is negative as long as θ_i is positive, and vice versa. This means that the product $F_y(\theta_i)\,\dot{y}_i$ is negative as long as $\text{sgn}(\theta_i) = \text{sgn}(\dot{y}_i)$. The sideways motion of a link is in other words contributing to the propulsion of the snake robot as long as θ_i is *positive during leftward motion of the link* (left with respect to the direction of motion) and *negative during rightward motion of the link* (right with respect to the direction of motion). This fundamental relationship may be written $\text{sgn}(F_{\text{prop},i}) = \text{sgn}(\text{sgn}(\theta_i)\,\text{sgn}(\dot{y}_i))$.

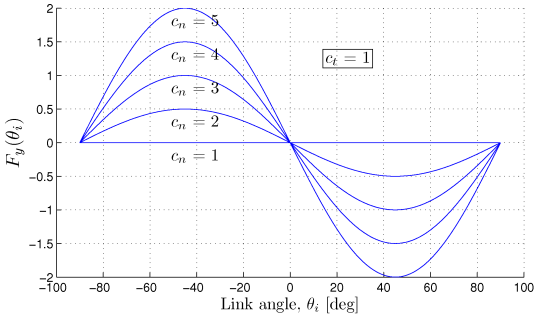

Fig. 4. The mapping from sideways link motion to forward propulsion for different viscous friction coefficients.

It is straightforward to calculate that the extrema of $F_y(\theta_i)$ occur at $\theta_i = \pm 45°$. This is also seen from Fig. 4. This means that, for a given $\dot{y}_i$, a link produces its highest propulsive force when it forms an angle of $\pm 45°$ with the forward direction of motion. It is also evident from (62) that the magnitude of $F_y(\theta_i)\,\dot{y}_i$, and thereby the magnitude of the propulsive force, $|F_{\text{prop},i}|$, is increased by increasing c_n with respect to c_t, or by increasing the magnitude of the sideways link velocity, $|\dot{y}_i|$.

It should now be clear that the function $F_y(\theta_i)$ *maps the link velocities normal to the direction of motion into force components in the direction of motion*. The following simple analogy may help understand this result. Imagine a small, hand-held, wheeled wagon of some sort. The direction of the wheels corresponds to the tangential direction of a snake robot link. Obviously, the friction coefficient of the wagon in the direction of the wheels is smaller than the friction coefficient normal to the wheels. Now assume that you push the wagon across a table in the direction of the wheels. While maintaining constant direction of motion, assume that you slowly rotate the wagon about the vertical axis, thereby forcing the wheels to slip. The hand that push and rotate the wagon will now feel a tendency of the wagon to move sideways in the same direction towards which the wagon was rotated. This is in accordance with the results presented above. The above analysis proves the following propositions:

Proposition 9: A planar snake robot with anisotropic ground friction properties achieves forward propulsion through the sideways (with respect to the forward direction) velocity components of its links.

Proposition 10: The direction of the propulsive force generated by the sideways motion of link i is given by the fundamental relationship $\text{sgn}(F_{\text{prop},i}) = \text{sgn}(\text{sgn}(\theta_i)\,\text{sgn}(\dot{y}_i))$.

Proposition 11: The function $F_y(\theta_i)$ maps the link velocities normal to the direction of motion into force components in the direction of motion.

Proposition 12: The magnitude of the propulsive force gen-

erated by link i, $|F_{\text{prop},i}|$, is increased by increasing c_n with respect to c_t, or by increasing the magnitude of the sideways link velocity, $|\dot{y}_i|$.

Proposition 13: For a given $\dot{y}_i$, a link produces its highest propulsive force when it forms an angle of $\theta_i = \pm 45^\circ$ with the forward direction of motion.

Note that these results are general in the sense that no assumptions have been made regarding the actual motion pattern displayed by the snake robot.

B. Synthesis of propulsive motion for the snake robot

The analysis from the previous section enables us to deduce how the snake robot links should be moved in order to propel the snake robot forward along the positive x axis. The following analysis focuses on manipulating the magnitude, $|F_{\text{prop},i}|$, and direction, $\text{sgn}\left(F_{\text{prop},i}\right)$, of the propulsive force from each link.

Theorem 3 in Section VI suggests that the angle of each link should be time-varying. Furthermore, Proposition 9 shows that propulsive forces are generated by moving the links in the *normal direction* with respect to the desired direction of motion. We therefore conclude that the links must have a *periodic* velocity component normal to the direction of motion. This suggests that each link should be moved alternatingly to the left and right with respect to the direction of motion, which can be achieved by letting the trajectory of each link angle have the form

$$\theta_i = \alpha \sin\left(\omega t\right), \quad i \in \{1, .., n\} \tag{64}$$

where $\alpha > 0$ is the maximum amplitude of the link angles during the locomotion, $\omega > 0$ is the angular frequency of the periodic motion, and t denotes time. For simplicity, we assume that α and ω are constant and identical for all links.

In accordance with Property 7 in Subsection VII-B, the joint angles should be *out of phase* during snake locomotion since this improves the controllability properties of the robot. This suggests that (64) should be modified to

$$\theta_i = \alpha \sin\left(\omega t + (i-1)\,\delta\right), \quad i \in \{1, .., n\} \tag{65}$$

where δ is the phase shift between adjacent links. For simplicity, we assume a constant phase shift between the links.

We now investigate how α, ω, and δ affect $|F_{\text{prop},i}|$ and $\text{sgn}\left(F_{\text{prop},i}\right)$ as the snake robot moves along the global x axis. To simplify the analysis, we assume that the snake robot consists of only $n = 3$ links. This is the minimum number of links required to achieve propulsion since phase shift between joints requires at least two joints. The below analysis for $n = 3$ links also apply to robots with $n > 3$ links since a snake robot can be regarded as a connection of multiple three-linked segments. The link angle trajectories are given from (65) as

$$\begin{aligned} \theta_1 &= \alpha \sin\left(\omega t\right) \\ \theta_2 &= \alpha \sin\left(\omega t + \delta\right) \\ \theta_3 &= \alpha \sin\left(\omega t + 2\delta\right) \end{aligned} \tag{66}$$

which, when differentiated with respect to time, gives the following angular link velocities:

$$\begin{aligned} \dot{\theta}_1 &= \alpha\omega \cos\left(\omega t\right) \\ \dot{\theta}_2 &= \alpha\omega \cos\left(\omega t + \delta\right) \\ \dot{\theta}_3 &= \alpha\omega \cos\left(\omega t + 2\delta\right). \end{aligned} \tag{67}$$

The normal direction velocity of each link is given from (14). We disregard the normal direction velocity of the snake robot by setting $\dot{p}_y \approx 0$. This approximation is a fairly accurate during motion along the global x axis, which is the case for this analysis. Inserting (66) and (67) into (14) gives

$$\begin{aligned} \dot{y}_1 = &-\tfrac{\alpha\omega l}{3}\left(2\cos\left(\omega t\right)\cos\left(\alpha\sin\left(\omega t\right)\right)\right) \\ &-\tfrac{\alpha\omega l}{3}\left(3\cos\left(\omega t + \delta\right)\cos\left(\alpha\sin\left(\omega t + \delta\right)\right)\right) \\ &-\tfrac{\alpha\omega l}{3}\left(\cos\left(\omega t + 2\delta\right)\cos\left(\alpha\sin\left(\omega t + 2\delta\right)\right)\right) \end{aligned} \tag{68}$$

$$\begin{aligned} \dot{y}_2 = &\tfrac{\alpha\omega l}{3}\left(\cos\left(\omega t\right)\cos\left(\alpha\sin\left(\omega t\right)\right)\right) \\ &-\tfrac{\alpha\omega l}{3}\left(\cos\left(\omega t + 2\delta\right)\cos\left(\alpha\sin\left(\omega t + 2\delta\right)\right)\right) \end{aligned} \tag{69}$$

$$\begin{aligned} \dot{y}_3 = &\tfrac{\alpha\omega l}{3}\left(\cos\left(\omega t\right)\cos\left(\alpha\sin\left(\omega t\right)\right)\right) \\ &+\tfrac{\alpha\omega l}{3}\left(3\cos\left(\omega t + \delta\right)\cos\left(\alpha\sin\left(\omega t + \delta\right)\right)\right) \\ &+\tfrac{\alpha\omega l}{3}\left(2\cos\left(\omega t + 2\delta\right)\cos\left(\alpha\sin\left(\omega t + 2\delta\right)\right)\right). \end{aligned} \tag{70}$$

Proposition 12 tells us that $|F_{\text{prop},i}|$ is increased by increasing $|\dot{y}_i|$. From (68)-(70), it is therefore clear that $|F_{\text{prop},i}|$ is increased by increasing α and/or ω. We now determine if δ should be positive or negative in order to achieve $\text{sgn}\left(F_{\text{prop},i}\right) = 1$, which is necessary to propel the snake robot forward along the global x axis. From Proposition 10, we know that $\text{sgn}\left(F_{\text{prop},i}\right) = 1$ requires $\text{sgn}\left(\theta_i\right) = \text{sgn}\left(\dot{y}_i\right)$. Considering $\dot{y}_2$ in (69) (since this expression is easy to analyze), it is seen through pure inspection that $\dot{y}_2 = 0$ when $\omega t = -\delta$. When $\omega t = -\delta$, we see from (66) and (67) that $\theta_2 = 0$ and $\dot{\theta}_2 = \alpha\omega > 0$. θ_2 is in other words about to become positive, which means that we also require $\dot{y}_2$ to become positive. This is the case if $\ddot{y}_2 > 0$ when $\omega t = -\delta$. Differentiating (69) with respect to time gives

$$\begin{aligned} \ddot{y}_2\big|_{\omega t = -\delta} = &\tfrac{2\alpha^2\omega^2 l}{3}\cos^2\left(\delta\right)\sin\left(\alpha\sin\left(\delta\right)\right) \\ &+\tfrac{2\alpha\omega^2 l}{3}\sin\left(\delta\right)\cos\left(\alpha\sin\left(\delta\right)\right) \end{aligned} \tag{71}$$

from which it is easily seen that $\ddot{y}_2 > 0$ when $\delta > 0$, i.e. $\text{sgn}\left(F_{\text{prop},i}\right) = 1$ when $\delta > 0$. This indicates that the links generate positive propulsive forces if $\delta > 0$.

In order to verify that forward propulsion requires $\delta > 0$, we have plotted (66) and (68)-(70) together in Fig. 5-7 for $\alpha = 70^\circ$, $\omega = 70^\circ$, and for different positive values of δ over a period of ωt from 0 to 2π. The figures show that $\text{sgn}\left(F_{\text{prop},i}\right) = \text{sgn}\left(\text{sgn}\left(\theta_i\right)\text{sgn}\left(\dot{y}_i\right)\right) = 1$ is always satisfied for link 2, but only satisfied over about half the period for links 1 and 3 when δ is small. As δ is increased, $\text{sgn}\left(F_{\text{prop},i}\right) = 1$ is satisfied over a larger portion of the period. We do not attempt to determine the optimal choice of δ in this analysis, but conclude that positive propulsive forces requires $\delta > 0$.

The above analysis proves the following propositions:

Proposition 14: A snake robot with anisotropic friction properties on a flat surface achieves forward propulsion by moving its links according to $\theta_i = \alpha \sin\left(\omega t + (i-1)\,\delta\right)$ where $i \in \{1, .., n\}$, $\alpha > 0$, $\omega > 0$, and $\delta > 0$.

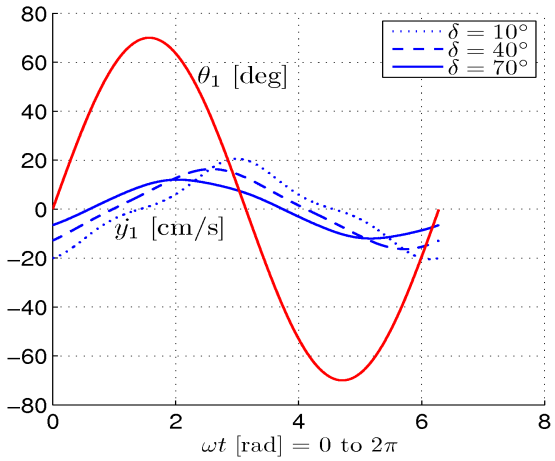

Fig. 5. The relation between θ_1 and $\dot{y}_1$ for $\alpha = 70°$, $\omega = 70°$, and $\delta = 10°$ (dotted) , $40°$ (dashed) , $70°$ (solid).

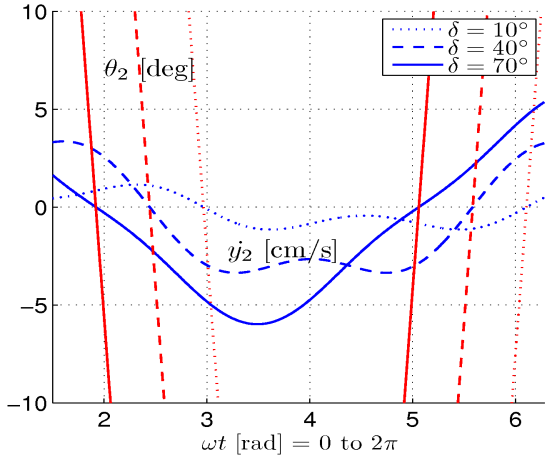

Fig. 6. The relation between θ_2 and $\dot{y}_2$ for $\alpha = 70°$, $\omega = 70°$, and $\delta = 10°$ (dotted) , $40°$ (dashed) , $70°$ (solid). The plot is zoomed in.

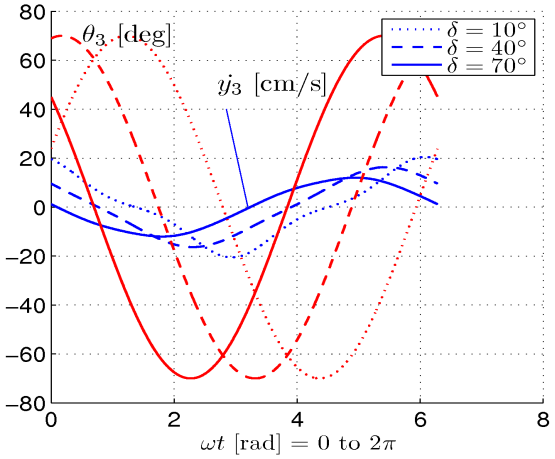

Fig. 7. The relation between θ_3 and $\dot{y}_3$ for $\alpha = 70°$, $\omega = 70°$, and $\delta = 10°$ (dotted) , $40°$ (dashed) , $70°$ (solid).

Proposition 15: Increasing α and/or ω increases the magnitude of the propulsive force generated by link i, $|F_{\text{prop},i}|$.

Note that the expression for the link angle trajectories in (65) has previously been deduced by Hirose [2] based on empirical studies of biological snakes. The above study shows that it is possible to develop logical arguments merely from an analysis of the equations of motion of a snake robot and thereby arrive at similar conclusions as Hirose.

IX. Path following control of snake robots

Based on the motion pattern developed in the previous section and summarized in Proposition 14, we propose in this section a control law for straight line path following control of snake robots. To this end, we define the global coordinate system so that the global x axis is aligned with the desired straight path. The position of the snake robot along the global y axis, p_y, is then the shortest distance from the robot to the desired path (i.e. the cross-track error) and the heading of the robot is the angle that the robot forms with the desired path.

Proposition 14 states that forward locomotion is achieved through sinusoidal motion of the n *absolute* link angles of the robot while maintaining a positive phase shift δ between adjacent links. However, since the snake robot is underactuated with only $n-1$ control inputs, it is not possible to control all n link angles independently. We therefore choose to control the $n-1$ *relative* joint angles (the angle of joint i is denoted by ϕ_i as described in Section IV-B) in order to generate a phase shifted sinusoidal motion of the n absolute link angles, and we introduce a joint angle offset in order to control the heading of the robot. The reference motion of ϕ_i is therefore given by

$$\phi_{i,\text{ref}} = \alpha \sin\left(\omega t + (i-1)\,\delta\right) + \phi_{\text{offset}} \tag{72}$$

where α, ω, and δ were defined in Section VIII-B, ϕ_{offset} is the joint angle offset, and $i \in \{1, .., n-1\}$. The offset is identical for all joints and affects the direction of the motion by making the link motion asymmetrical with respect to the current heading of the robot. This joint angle reference trajectory was first introduced in [2].

We denote the heading of the snake by $\overline{\theta}$ and calculate it as the mean of the link angles, i.e. as

$$\overline{\theta} = \frac{1}{n}\sum_{i=1}^{n} \theta_i. \tag{73}$$

In order to steer the snake robot towards the desired straight path (i.e. the global x axis), we employ the Line-of-Sight (LOS) guidance law

$$\overline{\theta}_{\text{ref}} = -\arctan\left(\frac{p_y}{\Delta}\right) \tag{74}$$

where p_y is the cross-track error, and $\Delta > 0$ is a design parameter referred to as the *look-ahead distance* that influences the rate of convergence to the desired path. This LOS guidance law is commonly used during e.g. path following control of marine surface vessels [32]. As illustrated in Fig. 8, the LOS angle $\overline{\theta}_{\text{ref}}$ corresponds to the orientation of the snake robot when it is headed towards the point located a distance Δ ahead of itself along the desired path. To steer the heading

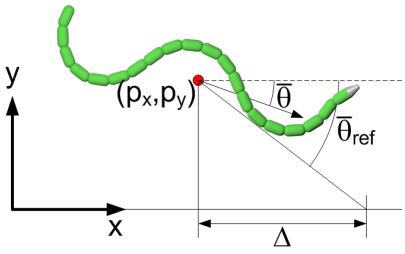

Fig. 8. The Line-of-Sight (LOS) guidance law.

$\overline{\theta}$ according to the LOS angle in (74), we set the joint angle offset according to

$$\phi_{\text{offset}} = k_\theta \left(\overline{\theta} - \overline{\theta}_{\text{ref}}\right) \tag{75}$$

where $k_\theta > 0$ is a controller gain. To make the joints track the reference angles given by (72), we use a PD-controller and set the actuator torque of joint $i \in \{1, .., n-1\}$ as

$$u_i = K_p \left(\phi_{i,\text{ref}} - \phi_i\right) - K_d \dot{\phi}_i \tag{76}$$

where $K_p > 0$ and $K_d > 0$ are controller gains, and where we have chosen to set $\dot{\phi}_{i,\text{ref}} = 0$ since the purpose of the derivative part is simply to damp the motion if the velocities become large.

X. Stability analysis of the path following controller based on the Poincaré map

In this section, we employ the theory of *Poincaré maps* (see Section III) to prove that the controller in (76) generates a *locally exponentially stable periodic orbit* in the state space of the snake robot as it moves along the global x axis.

A. Converting the snake robot model to a time-periodic autonomous system

During locomotion along the global positive x axis, our goal is that the x axis position of the snake robot, p_x, increases, while all other states of the snake robot in (26) trace out a stable limit cycle in the state space. We therefore exclude p_x from the Poincaré map of the snake robot. This corresponds to a *partial Poincaré map* [20]. Exclusion of p_x has no effect on the other state variables since p_x is not present in any of their derivatives in (26). The analysis of snake locomotion in Section VIII, which is the basis of the controller in (76), enables us to argue that forward motion along the x axis (increase of p_x) is achieved as long as the remaining state variables trace out a stable periodic orbit.

Stability analysis of the time-periodic state variables of the snake robot by use of Poincaré maps requires the model of the snake robot in (26) to represent an *autonomous* system, i.e. a system not explicitly dependent on time. The controller in (76), however, makes the system *non-autonomous* since time t is present in the expressions for the joint torque inputs. We therefore follow the approach described in [19] in order to convert the snake robot model to an autonomous system by simply augmenting the state vector x with an extra state $\beta = 2\pi t/T$, where $T = 2\pi/\omega$ is the period of the cyclic locomotion generated by the controller in (76). We make β periodic by enforcing that $0 \leq \beta < 2\pi$, i.e. we set β to zero each time $\beta = 2\pi$. The model (26) with the controller (76) can therefore be written as the following *autonomous* system:

$$\begin{array}{ll} \dot{x} = F\left(x, \frac{T}{2\pi}\beta\right), & x\left(t_0\right) = x_0, \\ \dot{\beta} = \frac{2\pi}{T}, & \beta\left(t_0\right) = \frac{2\pi t_0}{T}. \end{array} \tag{77}$$

We have, in other words, encapsulated time t in the new state variable β, which is periodic since $0 \leq \beta < 2\pi$.

B. Specification of the Poincaré section for the snake robot

We choose the global x axis as the *Poincaré section* $\mathcal{S}$ of the system in (77). Since p_x is not included in the Poincaré map, we write $\mathcal{S} = \left\{ \left(\theta, p_y, \dot{\theta}, \dot{p}, \beta\right) | p_y = 0 \right\}$. Following the notation in Section III, the vector of *independent* time-periodic states constrained to $\mathcal{S}$ is given by

$$\overline{x} = \begin{bmatrix} \theta^T & \dot{\theta}^T & \dot{p}^T & \beta \end{bmatrix}^T \in \mathbb{R}^{2n+3}. \tag{78}$$

Note that the considered Poincaré map is *one-sided*, i.e. the Poincaré section is crossed when p_y switches from a positive to a negative value.

C. Stability analysis of the Poincaré map

We considered a three-linked snake robot where $n = 3$, $l = 0.07$ m, $m = 1$ kg, and $J = 0.0016$ kgm^2. The ground friction coefficients were $c_t = 1$ and $c_n = 10$, and the parameters of the controller in (76) were $\alpha = 70°$, $\omega = 70°/s$, $\delta = 70°$, $K_p = 20$, $K_d = 5$, $k_\theta = 0.3$, and $\Delta = 0.42$ m.

The *Poincaré map* of the snake robot model in (77) was calculated as described in Section III-B1 using *Matlab R2008b* on a laptop running *Windows XP*. The *ode45* solver in Matlab was used with a relative and absolute error tolerance of 10^{-6}. The *Newton-Raphson algorithm* described in Section III-B2 calculated the *fixed point*, $\overline{x}^* \in \mathbb{R}^9$, of the Poincaré map as

$$\begin{array}{c} \overline{x}^* = [\ -15.0° \quad -32.6° \quad 27.6° \quad -72.4°/s \\ 13.7°/s \quad 66.7°/s \quad 4.6^{cm}/s \quad -1.2^{cm}/s \quad 182.5°\ ]^T. \end{array} \tag{79}$$

A plot of the cyclic locomotion of the snake robot over one period is shown in Fig. 9. The initial state of the snake robot was given by $\overline{x}^*$ and the initial position was $p = 0$. After one period of the motion, the state variables returned to their initial value, $\overline{x}^*$. At this point, however, the position of the snake robot along the x axis had increased, which was also our goal. To clearly illustrate the limit cycle behaviour of the periodic state variables in (78), a 3D plot of the three absolute link angles over one period is given in Fig. 10.

The Jacobian linearization of the Poincaré map about the fixed point (79) was calculated as described in Section III-B3. The magnitude of the eigenvalues of $J_P\left(\overline{x}^*\right) \in \mathbb{R}^{9\times 9}$ was

$$\begin{array}{c} |\text{eig}\left(J_P\left(\overline{x}^*\right)\right)| = [\ 0.78 \quad 0.78 \quad 0.0022 \\ 2.1 \times 10^{-4} \quad 4.9 \times 10^{-5} \quad 4.1 \times 10^{-5} \\ 9.6 \times 10^{-6} \quad 2.9 \times 10^{-6} \quad 1.6 \times 10^{-6}\ ]. \end{array} \tag{80}$$

The magnitude of all the eigenvalues are strictly less than one. The periodic orbit traced out by the variables in (78) is therefore *locally exponentially stable* for the given choice of controller parameters. All initial states inside the basin of

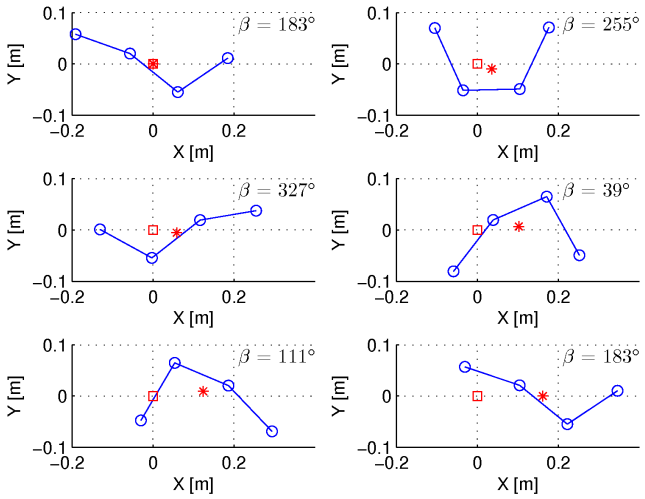

Fig. 9. The motion of the snake robot over one gait cycle.

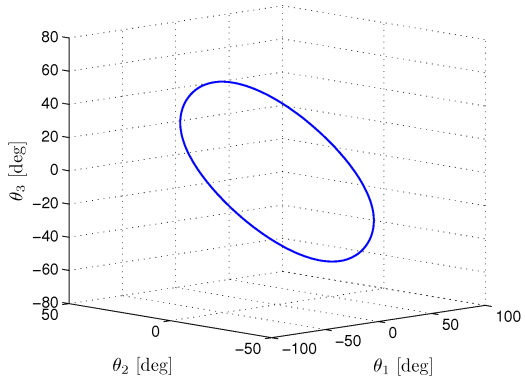

Fig. 10. The limit cycle traced out by the link angles of the snake robot.

attraction of this periodic orbit will converge *exponentially* to this periodic orbit.

We have now proven that the controller in (76) generates a stable periodic orbit comprising all state variables, except the position p_x. Based on the analysis in Section VIII, this implies that the snake robot is locomoting forward. In particular, Proposition 10 in Section VIII-A states that the direction of the propulsive force on the robot from link i is given by $\mathrm{sgn}\left(F_{prop,i}\right) = \mathrm{sgn}\left(\mathrm{sgn}\left(\theta_i\right)\mathrm{sgn}\left(\dot{y}_i\right)\right)$. A plot of θ_i and $\dot{y}_i$ $(i = 1, 2, 3)$ over one period is given in Fig. 11, which clearly shows that $\mathrm{sgn}\left(F_{prop,i}\right) = 1$ over the majority of the period. This means that the net propulsive force on the robot is positive.

XI. Conclusions

This paper has investigated the controllability and stability properties of planar snake robots influenced by viscous ground friction forces. The first contribution of the paper has been a partially feedback linearized model of a planar snake robot. The second contribution has been a stabilizability analysis proving that any asymptotically stabilizing control law for a planar snake robot to an equilibrium point must be *time-varying*. This result is valid regardless of which type of friction

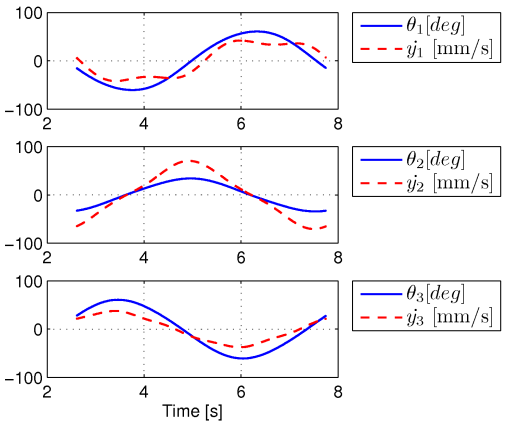

Fig. 11. Plot of θ_i and $\dot{y}_i$ $(i = 1, 2, 3)$ over one gait cycle.

the robot is subjected to. The third contribution has been a controllability analysis proving that planar snake robots are *not controllable* when the viscous ground friction is *isotropic*, but that a snake robot becomes *strongly accessible* when the viscous ground friction is *anisotropic*. This analysis showed that the joint angles of a snake robot should be *out of phase* during locomotion. The analysis also showed that the robot does *not* satisfy sufficient conditions for *small-time local controllability* (STLC). The fourth contribution has been an explanation of how anisotropic viscous ground friction conditions enable snake robots to locomote forward on a planar surface. The explanation was based on a simple mapping from link velocities *normal* to the direction of motion into *propulsive forces* in the direction of motion. The fifth and final contribution of the paper has been a straight line path following controller and the use of a *Poincaré map* to prove that the state variables of the robot, except for the position in the forward direction, trace out an *exponentially stable* periodic orbit during motion along the desired path.

References

[1] J. Gray, "The mechanism of locomotion in snakes," *J. Exp. Biol.*, vol. 23, no. 2, pp. 101–120, 1946.

[2] S. Hirose, *Biologically Inspired Robots: Snake-Like Locomotors and Manipulators*. Oxford: Oxford University Press, 1993.

[3] J. P. Ostrowski, "The mechanics and control of undulatory robotic locomotion," Ph.D. dissertation, California Institute of Technology, 1996.

[4] P. Prautsch and T. Mita, "Control and analysis of the gait of snake robots," in *Proc. IEEE Int. Conf. Control Applications*, Kohala Coast, HI USA, 1999, pp. 502–507.

[5] S. Ma, "Analysis of creeping locomotion of a snake-like robot," *Adv. Robotics*, vol. 15, no. 2, pp. 205–224, 2001.

[6] H. Date, M. Sampei, and S. Nakaura, "Control of a snake robot in consideration of constraint force," in *Proc. IEEE Int. Conf. on Control Applications*, 2001, pp. 966–971.

[7] M. Saito, M. Fukaya, and T. Iwasaki, "Serpentine locomotion with robotic snakes," *IEEE Contr. Syst. Mag.*, vol. 22, no. 1, pp. 64–81, February 2002.

[8] G. P. Hicks, "Modeling and control of a snake-like serial-link structure," Ph.D. dissertation, North Carolina State University, 2003.

[9] M. Nilsson, "Serpentine locomotion on surfaces with uniform friction," in *Proc. IEEE/RSJ Int. Conf. Intelligent Robots and Systems*, 2004, pp. 1751–1755.

[10] A. A. Transeth, N. van de Wouw, A. Pavlov, J. P. Hespanha, and K. Y. Pettersen, "Tracking control for snake robot joints," in *Proc. IEEE/RSJ Int. Conf. Intelligent Robots and Systems*, San Diego, CA, USA, Oct-Nov 2007, pp. 3539–3546.

[11] J. Li and J. Shan, "Passivity control of underactuated snake-like robots," in *Proc. 7th World Congress on Intelligent Control and Automation*, June 2008, pp. 485–490.
[12] M. Ishikawa, "Iterative feedback control of snake-like robot based on principal fiber bundle modeling," *Int. J. Advanced Mechatronic Systems*, vol. 1, no. 3, pp. 175–182, 2009.
[13] P. A. Vela, K. A. Morgansen, and J. W. Burdick, "Underwater locomotion from oscillatory shape deformations," in *Proc. IEEE Conf. Decision and Control*, vol. 2, Dec. 2002, pp. 2074–2080 vol.2.
[14] K. McIsaac and J. Ostrowski, "Motion planning for anguilliform locomotion," *IEEE Trans. Rob. Aut.*, vol. 19, no. 4, pp. 637–625, 2003.
[15] K. Morgansen, B. Triplett, and D. Klein, "Geometric methods for modeling and control of free-swimming fin-actuated underwater vehicles," *IEEE Trans. Robotics*, vol. 23, no. 6, pp. 1184–1199, Dec 2007.
[16] P. Liljebäck, K. Y. Pettersen, Ø. Stavdahl, and J. T. Gravdahl, "Controllability analysis of planar snake robots influenced by viscous ground friction," in *Proc. IEEE/RSJ Int. Conf. Intelligent Robots and Systems*, 2009, pp. 3615–3622.
[17] ——, "Stability analysis of snake robot locomotion based on Poincaré maps," in *Proc. IEEE/RSJ Int. Conf. Intelligent Robots and Systems*, 2009, pp. 3623–3630.
[18] P. Liljebäck, K. Y. Pettersen, and Ø. Stavdahl, "Modelling and control of obstacle-aided snake robot locomotion based on jam resolution," in *Proc. IEEE Int. Conf. Robotics and Automation*, 2009, pp. 3807–3814.
[19] T. S. Parker and L. O. Chua, *Practical Numerical Algorithms for Chaotic Systems*. Springer-Verlag, 1989.
[20] E. R. Westervelt, J. W. Grizzle, C. Chevallereau, J. H. Choi, and B. Morris, *Feedback Control of Dynamic Bipedal Robot Locomotion*. CRC Press, 2007.
[21] H. Nijmeijer and A. v. d. Schaft, *Nonlinear Dynamical Control Systems*. New York: Springer-Verlag, 1990.
[22] H. J. Sussmann, "A general theorem on local controllability," *SIAM Journal on Control and Optimization*, vol. 25, no. 1, pp. 158–194, 1987.
[23] R. M. Bianchini and G. Stefani, "Graded approximations and controllability along a trajectory," *SIAM J. Control and Optimization*, vol. 28, no. 4, pp. 903–924, 1990.
[24] Y.-L. Gu and Y. Xu, "A normal form augmentation approach to adaptive control of space robot systems," in *Proc. IEEE Int. Conf. Robotics and Automation*, vol. 2, May 1993, pp. 731–737.
[25] M. W. Spong, "Partial feedback linearization of underactuated mechanical systems," in *Proc. IEEE/RSJ/GI Int. Conf. Intelligent Robots and Systems*, vol. 1, 1994, pp. 314–321.
[26] M. Reyhanoglu, A. van der Schaft, N. McClamroch, and I. Kolmanovsky, "Dynamics and control of a class of underactuated mechanical systems," *IEEE Transactions on Automatic Control*, vol. 44, no. 9, pp. 1663–1671, September 1999.
[27] H. Goldstein, C. Poole, and J. Safko, *Classical Mechanics - Third Edition*. Addision Wesley, 2002.
[28] R. Brockett, "Asymptotic stability and feedback stabilization," *Differential Geometric Control Theory*, pp. 181–191, 1983.
[29] J.-M. Coron and L. Rosier, "A relation between continuous time-varying and discontinuous feedback stabilization," *J. of Mathematical Systems, Estimation, and Control*, vol. 4, no. 1, pp. 67–84, 1994.
[30] D. A. Harville, *Matrix Algebra From a Statistician's Perspective*. Springer, 2000.
[31] T. Kane and D. Lecison, "Locomotion of snakes: A mechanical 'explanation'," *Int. J. Solids Struct.*, vol. 37, no. 41, pp. 5829–5837, 2000.
[32] T. I. Fossen, *Marine Control Systems: Guidance, Navigation and Control of Ships, Rigs and Underwater Vehicles*. Trondheim, Norway: Marine Cybernetics, 2002.

Pål Liljebäck (M'08) received the MSc degree from the Department of Engineering Cybernetics, Norwegian University of Science and Technology (NTNU), Trondheim, Norway, in 2004. He is currently a PhD student at this department at NTNU, and simultaneously works as a research scientist at SINTEF ICT, Department of Applied Cybernetics, Trondheim, Norway, which is a Norwegian research organization. His research interests include modelling and control of dynamical systems, and design and implementation of mechatronic systems.

Kristin Y. Pettersen (S'93–M'98–SM'04) received her MSc and PhD degree in Electrical Engineering at the Norwegian University of Science and Technology (NTNU), Trondheim, Norway, in 1992 and 1996 respectively. In 1996 she became Associate Professor, and in 2002 Professor, at the Department of Engineering Cybernetics, NTNU. In 1999 she was a Visiting Fellow at the Department of Mechanical and Aerospace Engineering, Princeton University, Princeton, NJ and in 2008 Visiting Professor at Section for Automation and Control, University of Aalborg, Denmark. She has published more than 100 conference and journal papers. In 2006 she received the IEEE Transactions on Control Systems Technology Outstanding Paper Award. She is a senior member of IEEE and Associate Editor of the IEEE Transactions on Control Systems Technology. She furthermore holds several board positions in industrial and research companies. Her research interests include nonlinear control of mechanical systems with applications to robotics, satellites, AUVs and ships.

Øyvind Stavdahl (M'09) was born in Lillehammer, Norway, 1967. He received the MSc and PhD from the Department of Engineering Cybernetics, Norwegian University of Science and Technology (NTNU), Trondheim, Norway, in 1994 and 2002, respectively. He became a Research Scientist in 1998 and in 2004 a Senior Scientist at SINTEF ICT, Department of Applied Cybernetics, where he currently is a Scientific Advisor. In 2004 he became a Postdoctoral Fellow, in 2007 Lecturer and in 2008 Associate Professor at the Department of Engineering Cybernetics, NTNU. In 2005 he was a Visiting Fellow at the Institute of Biomedical engineering, University of New Brunswick, Fredericton, NB, Canada. Dr. Stavdahl is a Board Member of the Norwegian Association of Automatic Control. His research interests include rehabilitation engineering, human movement analysis and biomimetic robotics.

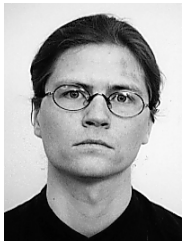

Tommy Gravdahl (S'94–M'98–SM'04) graduated siv.ing (1994) and dr.ing (1998) in engineering cybernetics at the Norwegian University of Science and Technology (NTNU), Trondheim, Norway. He was appointed Associate Professor (2001) and Professor (2005) at the Department of Engineering Cybernetics, NTNU. In the academic year 2007/08 he was Visiting Professor with The Centre for Complex Dynamic Systems and Control (CDSC), The University of Newcastle, Australia. He has published more than 75 papers at conferences and in journals and is author of Compressor Surge and Rotating Stall: Modeling and Control (London, Springer, 1999), co-author of Modeling and Simulation for Automatic Control (Trondheim, Marine Cybernetics, 2002) and co-editor of Group Coordination and Cooperative Control (Berlin, Springer, 2006). His research interests include mathematical modeling and nonlinear control in general, modeling and control of turbomachinery and control of spacecraft, robots and nanopositioning devices. Professor Gravdahl received the IEEE Transactions on Control Systems Technology Outstanding Paper Award in 2000 and is member of the editorial board of Simulation Modeling Practice and Theory.